KfK 3279
EUR 7057e
Mai 1982

A Critical Heat Flux Correlation for Advanced Pressurized Light Water Reactor Application

M. Dalle Donne, W. Hame
Institut für Neutronenphysik und Reaktortechnik
Projekt Schneller Brüter

Kernforschungszentrum Karlsruhe

KERNFORSCHUNGSZENTRUM KARLSRUHE

Institut für Neutronenphysik und Reaktortechnik
Projekt Schneller Brüter

KfK 3279
EUR 7057e

A critical heat flux correlation for Advanced Pressurized Light Water Reactor application

M. Dalle Donne[+], W. Hame[++]

[+]) Delegated from Euratom to the Karlsruhe Nuclear Research Center, Institute for Neutron Physics and Reactor Engineering.

[++]) Ingenieurbüro für Programmentwicklung in Thermo- und Fluiddynamik

Kernforschungszentrum Karlsruhe GmbH, Karlsruhe

Kernforschungszentrum Karlsruhe GmbH
ISSN 0303-4003

Abstract

Many CHF-correlations have been developed for water cooled rod clusters representing typical PWR or BWR fuel element geometries with relative wide rod lattices. However the fuel elements of an Advanced Pressurized Water Reactor (APWR) have a tight fuel rod lattice, in view of increasing the fuel utilization. It was therefore decided to produce a new CHF-correlation valid for rod bundles with tight lattices. The already available WSC-2 correlation was chosen as a basis. The geometry dependent parameters of this correlation were determined again with the method of the root mean square fitting from the experimental data of the CHF-tests performed in the frame of the Light Water Breeder Reactor programme at the Bettis Laboratory. These tests include triangular array rod bundles with very tight lattices. Furthermore the effect of spiral spacer ribs was investigated on the basis of experimental data from the Columbia University. Application of the new CHF-correlation to conditions typical for an APWR shows that the predicted critical heat fluxes are much smaller than those calculated with the usual PWR-CHF-correlations, but they are higher than those predicted by the B&W-VPI&SU correlation.

Eine neue kritische Heizflächenbelastungskorrelation zur Anwendung beim Fortgeschrittenen Druckwasser-Reaktor

Zusammenfassung

Für die bei herkömmlichen Druckwasser- und Siedewasserreaktoren üblichen Brennelementbündel mit verhältnismäßig großer Stabteilung sind eine Vielzahl von Beziehungen zur Berechnung des kritischen Wärmeflusses bekannt. Die Brennelemente eines fortgeschrittenen Druckwasserreaktors haben jedoch - im Hinblick auf eine Erhöhung der Brennstoffausnutzung - eine enge Stabteilung. Es war deshalb erforderlich, für solche enge Stabgitter eine neue Beziehung für den kritischen Wärmefluß aufzustellen. Auf der Basis der bereits vorhandenen WSC-2-Beziehung wurden die geometrieabhängigen Parameter in der Funktionsgleichung nach der Methode der kleinsten Quadrate neu bestimmt. Die Meßdaten für die Anpassung der Parameter wurden den Ergebnissen der Versuche zur Bestimmung des kritischen

Wärmeflusses entnommen, die im Rahmen eines Leichtwasser-Brutreaktor-Programms am Bettis-Laboratorium durchgeführt wurden. In diesen Versuchsreihen waren auch Messungen an Stabbündeln mit sehr geringer Teilung durchgeführt worden. Außerdem wurde der Einfluß von wendelförmigen Abstandshaltern auf den kritischen Wärmefluß auf der Basis von Experimenten der Columbia University bestimmt. Die Anwendung der neuen Beziehung auf eine FDWR-spezifische Anordnung zeigt, daß der zu erwartende kritische Wärmefluß beträchtlich unter dem Wert liegt, der mit den für Druckwasserreaktoren üblichen Beziehungen berechnet wird. Jedoch liegt der kritische Wärmefluß höher als die Vorhersage der B&W-VPI&SU-Korrelation.

1. Introduction

Recently the Karlsruhe Nuclear Research Center and Kraftwerk Union in collaboration with the Technical University of Braunschweig have started an investigation on the possibility of increasing the conversion ratio of a pressurized light water reactor in view of improving uranium utilisation |1,2,3|. The fuel element is based on UO_2-PuO_2 fuel, where the plutonium vector for the fresh fuel is given by the fuel discharged from a Light Water Reactor. Two types of fuel elements are being investigated: a modular core formed by hexagonal fuel elements containing an external blanket with lower enrichment and an internal seed with higher enrichment |1|,and a homogeneous core where all the rods in the core have the same diameter |2|.

For both alternatives the water volume fraction in the core must be considerably smaller than in a PWR, thus the neutron spectrum becomes harder and the conversion ratio higher. This means that for an Advanced Pressurized Light Water Reactor (APWR) the fuel rod lattice must be tighter than in a PWR.
In the frame of the fluid- and thermodynamic calculation programme for the APWR |4| it was felt that a new critical heat flux correlation was required, better suited to the fuel element geometry considered than the already existing CHF-correlations.

2. Existing CHF-correlations

Many CHF-correlations have been developed for water cooled rod clusters representing typical PWR and BWR fuel element geometries. Table I+ gives a resumê of the correlations, most recent and/or most relevant to our particular case. All these correlations are valid for rod cluster geometries, with the exception of the Shippingport correlation which is based on experiments with water flow in thin rectangular channels |5| . This correlation is quoted here because in the Light Water Breeder Reactor Safety Report |6| it is stated

+British thermal units are used in the present paper, because all the correlations used in the present paper are in those units. Appendix I of the paper gives the unit conversion factors of the main physical parameters.

that it has been qualified by the CHF tests performed at the Bettis Laboratory for the LWBR for tight lattices as well. The correlations of references |7| to |10| have been developed for typical LWR fuel element geometries, i.e. for bundles with wider lattices than those relevant to the reactor type under consideration in the present paper. The B&W-VPI&SU correlation |11| was developed especially for a tight lattice (validity down to a hydraulic diameter D_h of the coolant channel equal to 0.14 in) however the extrapolation to small coolant channel hydraulic diameters has been based on a rather limited experimental evidence. Furthermore the effect of spiral spacer ribs usually present in fuel rod bundles with very tight lattices has not been investigated.

Table II shows the experimental data on which the B&W-VPI&SU correlation is based. Reference |12| reports on tests performed on a single channel, whose form simulates a flow channel within a bundle of closely spaced rods ($D_h \approx$ 0.15 in). The data of reference |14| were used to test the correlation with data obtained for non-uniform axial flux shape, although these data were obtained for a relative wide lattice. Only the data from reference |13| refer to rod clusters with tight lattices, however only 148 data are used of the total 528 available from this work. This because only the data points within the range of mass velocity between 1.0×10^6 and 4.0×10^6 lb/hr ft^2 and for the test sections uniformly heated in radial direction were used for establishing the B&W-VPI&SU correlation.

Table III shows the CHF predictions with the various correlations for two typical APWR applications: a homogeneous and the seed part of a heterogeneous reactor |4|. X is the steam quality at the CHF point. As usual X negative means subcooling. The discrepancies are rather large. As expected, the PWR correlations predict too high values expecially in the case of low D_h (homogeneous reactor). This is due to the fact that the correlations of references |7| to |9| have been developed for PWR fuel elements, i.e. for higher coolant channel hydraulic diameters and for less negative local steam qualities (see Table 1). Only the quite recent WSC-2 correlation agrees reasonably well with the B&W-VPI&SU correlation, especially developed for tight lattices. Furthermore the WSC-2 is rather flexible in its application, because it is possible to separate its empirical

parameters which depend upon the geometry of the bundle from the others. However, the WSC-2 correlation has not been especially developed for tight lattices and it was therefore decided to determine its geometry-dependent parameters again on the base of the CHF-tests performed for triangular array rod clusters |13,15,16|.

The WSC-2 is based on experiments performed with rod clusters with grid spacers. The experimental evidence of reference |10| and from Westinghouse as well |17| indicates that the presence of spacer grids augments the initial heat flux and that this effect increases about linearly with the coolant mass velocity G. The fuel rods of a homogeneous reactor and those of the blanket of a heterogeneous one are spaced by spiral ribs. These should have an even greater effect on the critical heat flux, because the spiral ribs are all over the length of the cluster, while the spacer grids are placed in discrete positions along the length of the cluster, thus the departure from nucleate boiling occurs generally away from the grids. Therefore in the present work we try to determine the effect of the spiral rib spacers as well. This was possible by the use of the experimental data of reference |18|, which reports the results of CHF-experiments performed at the Columbia University with a triangular array rod bundle with a tight lattice and with spiral spacers.

3. The present CHF-correlation

3.1 Experimental data base

Table IV shows the WSC-2 correlation where Q_1, Q_2 and Q_4 are the geometry dependent parameters. In the WSC-2 correlation for a rod cluster with a triangular array, they are given as $Q_1 = 1.329$, $Q_2 = 2.372$ and $Q_4 = 12.26$. For the best fit of the experimental data with grid spacers, Bowring suggests to use for the term V, which accounts for the spacer effect, the constant value 0.7 |10|. Objective of the present work was to establish new Q_1, Q_2, Q_4 and V values based on the experimental data of references |13,15,16| and |18|. All these data points refer to critical heat flux experiments performed with triangular array rod clusters either at the Bettis Laboratory in the frame of the Light Water Breeder Reactor programme or at the Columbia University. Some of the Bettis data were used for the B&W-VPI&SU correlation (148 data points), however in the present work a considerably greater experimental evidence was used (695 data points for rod clusters with grid spacers and 44 data points for the rod cluster with spiral rib spacers).

Table V shows the data of the experimental evidence on which the present correlation is based. We considered not only uniform transversal heat flux distribution, but also experiments with a radial non-uniform power distribution in the rods. This is taken into account by the radial form factor F_p which appears in the WSC-2 correlation. Furthermore also the tests with mass velocities smaller than 10^6 lb/ft^{2}hr were considered.

Aim of the present work is to produce a CHF-correlation valid for the central coolant channels of a cluster. Generally the burn-out does not occur in the wall or corner channels of the cluster of fuel rods, because there the water temperature is lower than in the central channels. The mass velocity G in the references |13,15,16| and |18| is the average for the whole bundle inclusive of wall and corner channels. Because the number of rods in these tests is relatively small (20 for the tests at Bettis, 12 for the tests at Columbia) the effect of the wall and corner channels could not be negligible. We decided therefore to correct the given average $\overline{G}$ values, to obtain G values for the central channels of the clusters. Assuming uniform water density, constant friction factors and equal pressure drop in the various coolant channels, one obtains the correction factor:

$$F_G = \frac{G}{\overline{G}} = \frac{(nA + n_w A_w + n_c A_c)\sqrt{D_h}}{nA\sqrt{D_h} + n_w A_w \sqrt{D_{hw}} + n_c A_c \sqrt{D_{hc}}} \qquad (1)$$

where n, n_w, n_c is the number of the central, wall and corner channels, and A, A_w, A_c and D_h, D_{hw}, D_{hc} are the cross section areas and hydraulic diameters of the central, wall and corner channels respectively. When the correction factor F_G was more than 10 % different from one, it was decided not to use the relative experimental evidence. In practice this lead to the exclusion of only one test section (Test 2A without "protrusious" of ref. |15|) for which F_G = 0.8877. The data of this test are reported here (Table 14), however they have not been used for the present correlation. In section 3.3.4 we shall see how well our correlation agrees with these data. For the data from the Columbia University it was assumed F_G = 1, because the hydraulic diameters of the corner and wall channels are about the same as that of the central channels, furthermore the strong radial coolant mixing caused by the spiral spacers ensures that the mass velocity is same in the various coolant channels. At the end of the paper the experimental data for the data points from Bettis |Tables 1 to 13| and from Columbia |Table 15| used for the present correlation are given together with the values of the

parameters used in the present computation. The mass velocities in the tables are the uncorrected average $\bar{G}$-values.

3.2 Method of calculation

For the determination of the geometry dependent parameters Q_1, Q_2, and Q_4 the WSC-2 CHF-correlation is used in the following formulation

$$\phi = \frac{K_1 Q_1}{(1+K_2 Q_2)(K_3+K_4 Q_4)} + \frac{K_o}{K_3+K_4 Q_4} \qquad (2)$$

The coefficients K_o, K_1, K_2, K_3, and K_4 are determined by the experimental data:

$$K_o = \frac{1}{4} G \cdot D \cdot \Delta Hi \qquad (3)$$

$$K_1 = \frac{1}{4} G \cdot D \cdot \lambda \cdot F_1 \qquad (4)$$

$$K_2 = G \cdot D \cdot F_2 \qquad (5)$$

$$K_3 = Z \cdot Y \qquad (6)$$

$$K_4 = V \cdot \left(1+\frac{(Y-1)}{1+G}\right) \cdot F_3 \cdot \frac{\sqrt{G\ D}}{D_h} \qquad (7)$$

(For an explanation of the symbols see Table IV).

The functions F_1, F_2, and F_3 depend on the pressure, and G, D, D_h, V, Y, Z are the mass flow velocity and geometric coefficients respectively (Table IV). ΔHi is the inlet subcooling and λ the heat of evaporation. The critical heat flux ϕ, the measured value, is used to determine the constants Q_1, Q_2, and Q_4 so that the euklidian Norm of the related error is a minimum:

$$e_i = \frac{1}{\phi_i} \left(\phi_i - \frac{K_{1i} Q_i}{(1+K_{2i} Q_2)(K_{3i}+K_{4i} Q_4} - \frac{K_{oi}}{K_{3i}+K_{4i} Q_4}\right) \qquad (8)$$

The index "i" in this equation denotes the coefficients computed from a single experiment. The Norm of the vector e_i is then given by

$$N = \|e_i\| = \sum_i e_i^2 \qquad (9)$$

and the necessary conditions for a minimum are

$$\frac{\partial N}{\partial Q_1} = \frac{\partial N}{\partial Q_2} = \frac{\partial N}{\partial Q_4} = 0. \tag{10}$$

From equations (10) follows a system of three nonlinear algebraic equations

$$\begin{aligned} f_1(Q_1, Q_2, Q_4) &= 0; \\ f_2(Q_1, Q_2, Q_4) &= 0; \\ f_3(Q_1, Q_2, Q_4) &= 0; \end{aligned} \tag{11}$$

which can be solved by the Newton-Raphson-Method

$$\underline{f} + \underline{f}' \cdot \underline{\delta Q} = 0 \tag{12}$$

The vector $\underline{f}^T = \{f_1, f_2, f_3\}$ is the function from equation (10) and f' denotes the matrix

$$\underline{f}' = \begin{vmatrix} \frac{\partial f_1}{\partial Q_1} & \frac{\partial f_1}{\partial Q_2} & \frac{\partial f_1}{\partial Q_4} \\ \frac{\partial f_2}{\partial Q_1} & \frac{\partial f_2}{\partial Q_2} & \frac{\partial f_2}{\partial Q_4} \\ \frac{\partial f_3}{\partial Q_1} & \frac{\partial f_3}{\partial Q_2} & \frac{\partial f_3}{\partial Q_4} \end{vmatrix} \tag{13}$$

If $\underline{Q}^T = \{Q_1, Q_2, Q_4\}$ is an initial guess, then an improved solution can be obtained from

$$\underline{Q}^1 = \underline{Q}^0 - (\underline{f}'(Q^0))^{-1} \cdot \underline{f}(Q^0) \tag{14}$$

and as in the usual Newton-method this procedure can be repeated

$$\underline{Q}^{\nu+1} = \underline{Q}^{\nu} - (f'(Q^{\nu}))^{-1} \cdot \underline{f}(Q^{\nu}) \tag{15}$$

until the difference

$$d = \| \underline{Q}^{\nu+1} - \underline{Q}^{\nu} \| \tag{16}$$

is as small as desired. The convergence of this algorithm depends on the matrix $\underline{f}'$ and the method cannot be used, if $\underline{f}'$ is singular or ill-conditioned in the surrounding of a solution $\underline{Q}$. In our problem nearly in all cases the matrix $\underline{f}'$ proved to be very ill-conditioned and so another method had to be chosen.

This method consists of two steps. The first step is to find a rough guess $\underline{Q}^o$ of the solution by searching the minimum value of N for discrete values of $\underline{Q}$

$$\begin{aligned} Q_1 &= (i-1)\ \delta Q_1 + Q_{10}; \\ Q_2 &= (j-1)\ \delta Q_2 + Q_{20}; \\ Q_4 &= (k-1)\ \delta Q_4 + Q_{40}; \end{aligned} \tag{17}$$

In this point $\underline{Q}^o$ the gradient of the function N is computed

$$\nabla^T N(\underline{Q}^o) = \{\frac{\partial N}{\partial Q_1}, \frac{\partial N}{\partial Q_2}, \frac{\partial N}{\partial Q_4}\} \tag{18}$$

and used as the advancing direction in the second step

$$\underline{Q}^1 = \underline{Q}^o + \alpha \cdot \nabla N \tag{19}$$

The parameter α is determined from the following condition

$$\nabla^T N(\underline{Q}^1) \cdot \nabla N(\underline{Q}^o) \approx 0. \tag{20}$$

This means, that the new direction $\nabla N(\underline{Q}^1)$ is chosen nearly perpendicular to the direction $\nabla N(\underline{Q}^o)$ of the previous step. The procedure is repeated until

$$d = \| \nabla N \| = \nabla^T \cdot N(\underline{Q}^\nu) \cdot \nabla N(\underline{Q}^\nu) \tag{21}$$

is less then a given positive number δ. Equations (19) and (20) were solved by finding the value α for which

$$\nabla^T N(\underline{Q}^1) \cdot \nabla N(\underline{Q}^o)$$

changes the sign. A method of interval bisecting was used.

Since in all our cases the function $N(Q_1, Q_2, Q_4)$ is of elliptic type in the entire domain, this method always converged. The solution was improved, until the Norm of the gradient was less then 10^{-12}.

As a measure for the least square fit and the computed parameters Q_1, Q_2, and Q_4, the mean error, the standard deviation and the root mean square error are determined from the following equations:

mean error:
$$\bar{e} = \frac{1}{n} \sum_{i=1}^{n} e_i \tag{22}$$

standard deviation:
$$\sigma = \sqrt{\frac{1}{n-1} \sum_{i=1}^{n} (e_i - \bar{e})^2} \tag{23}$$

RMS-error:
$$\varepsilon_{RMS} = \sqrt{\frac{\sum_{i=1}^{n} e_i^2}{n}} \tag{24}$$

The programm CHF is written in FORTRAN IV. It computes the values of Q_1, Q_2, Q_4 from a maximum of (at this stage) 1000 experimental data points following the described manner. In addition certain options can be chosen:

- minimizing of the absolute square sum

$$E_i = \phi_i \cdot e_i \tag{25}$$

- omitting of certain data points
  such as all experiments with $G < 10^6$
- plotting of the computed values versus the measured values.

The internal parameters of the algorithm such as increments δQ_i, and $\delta\alpha$ or the value δ are defined so that in all considered cases solutions were obtained after a few steps (ten to twenty).

3.3 Calculation results

3.3.1 Calculations with V = 0.7. Bettis data

Originally we performed our calculations for the Bettis data using V = 0.7, which is the best fit value recommended by Bowring for clusters with PWR-typical grid spacers |10|. Fig. 1 shows the result of these calculations in the form $\psi = \phi_{comp.}/\phi_{exp.}$ versus the mass velocity G. (The dotted region is one standard deviation wide). From the figure it is evident that a systematic G-effect is still present: on average the ratio ψ decreases with G. The most likely cause of this is that, with V = 0.7, we underestimate the effect of the grid spacers on the critical heat flux at high mass velocities. This seems reasonable, because in presence of coolant channels with smaller hydraulic diameters than those of a PWR, the effect of the spacers should be greater on the pressure drop and thus on the critical heat flux, due to the greater obstruction caused by the spacers themselves. We decided therefore to try to find a function V = V(G) capable of eliminating this G-effect on the computed critical heat flux.

3.3.2 Calculations with variable V. Bettis data: grid spacers

Fist of all we performed a calculation with V = 1. This V-value corresponds to the case of clusters with relatively non-obstructive spacers or without spacers |10| and by using V = 1 we try to put in evidence what is the effect of the spacer grids on the critical heat flux. Fig. 2 shows the results of these calculations in the form ψ versus G. The values of the parameters Q are:

$$\begin{aligned} Q_1 &= 1.763 \\ Q_2 &= 9.157 \\ Q_4 &= 6.507 \end{aligned} \qquad (26)$$

While the mean error, the standard deviation and the RMS-error are respectively:

$$\begin{aligned} \bar{e} &= -1.97\% \\ \sigma &= 13.75\% \\ \varepsilon_{RMS} &= 13.89\% \end{aligned} \qquad (27)$$

Fig. 3 shows the V-values versus G. These V-values have been calculated with the Q-values of equation (26) and the experimental values of the critical heat flux. The points scatter quite considerably, due to the magnification effect between Φ_{CHF} and V inplicit in the WSC-2 correlation, however a systematic effect is visible. This can be best approximated by the following equation:

$$V = 3.1 - 1.15\ G + 0.1138\ G^2 - 2.5\ \exp(-G) \qquad (28)$$

which is plotted in Fig. 3 as well.

Fig. 4 shows the results of a new calculation using the Q-values of equation (26) and V from equation (28). The systematic G-effect has been eliminated. The mean error, the standard deviation and the RMS-error are respectively:

$$\begin{aligned} \bar{e} &= -0.79\% \\ \sigma &= 12.71\% \\ \varepsilon_{RMS} &= 12.73\% \end{aligned} \qquad (29)$$

Fig. 5 shows the same data of Fig. 4 in the plot computed ϕ_{CHF} versus experimental ϕ_{CHF} and Fig. 6 in the plot $\psi = \phi_{CHFcomp.}/\phi_{CHFexp.}$ versus $\phi_{CHFexp.}$.

3.3.3 Calculations with variable V: Columbia data: spiral rib spacer

Fig. 7 shows the results of the calculation with the Columbia experimental data (Table 15) obtained with a cluster with spiral rib spacers. Plotted is $\psi = \phi_{CHFcomp.}/\phi_{CHFexp.}$ versus G. The computed ϕ_{CHF}-values are obtained with the Q-values of eq. (26) and V = 1. From the figure it is evident that the computed ϕ_{CHF}-values are much too low, especially at the high G-values. As expected the spiral rib spacers have a considerable higher effect on the critical heat flux than the spacer grids (s. section 2).

Fig. 8 shows the V-values, calculated with the Q-values of eq. (26) and the experimental values of ϕ_{CHF}, versus G. The points may be correlated by the equation:

$$V = 1 - \left[0.25 + 0.1\ G + 2.75\ \exp(-4\ G) - 3\ \exp(-3G)\right] \qquad (30)$$

which is plotted on Fig. 8 as well. Eq. (30) is such that for G = 0, V = 1. This is not necessarily dictated by the experimental points and was simply assumed, because for low G-values the effect of the spacers should be small (clusters with non-obstructive spacers: V = 1 |10|), and also because this makes the application of the correlation easier (s. Section 3.4).

Fig. 9 shows the results of a new calculation using the Q-values of equation (26) and V from equation (29). The systematic G-effect has been eliminated. The mean error, the standard deviation and the RMS-error are respectively:

$$\begin{aligned} \bar{e} &= -0.07\% \\ \sigma &= 6.18\% \\ \varepsilon_{RMS} &= 6.18\% \end{aligned} \qquad (31)$$

Fig. 10 shows the same data of Fig. 9 in the plot computed ϕ_{CHF} versus experimental ϕ_{CHF}.

3.3.4 Effect of wall and corner channels: the factor F_G

As we mentioned already in section 3.1, we corrected the mass velocity G to try to eliminate the effect of the wall and corner channels on the critical heat flux. This was done with the correction factor F_G (see eq. (1)). The greatest value of F_G used for the present calculation was F_G = 1.0686 for the data of Tables 1 and 2 (ref. |15|). To assess the effect of this correction, we evaluated with the present correlation the data of Table 1 and 14, both from ref. |15|, which have quite different F_G-values (in the case of the data of Table 14 F_G = 0.8877, but these data were not used to obtain our correlation), buth otherwise the same geometrical parameters and the same power distribution: in fact these tests were performed with the same test section placed in two different shrouds, where for the tests of Table 1 protrusions were placed in the wall channels to reduce the large differences in hydraulic diameter between central (D_{hc} = 0.11 cm) and wall channels (D_{hw} = 0.169 cm). By the presence of the protrusions the wall channel hydraulic diameter was reduced to the value of D_{hw} = 0.084 cm.

Fig. 11 shows the data of Table 1 in the plot ψ versus mass velocity G. The present correlation (equations (26) and (28)) predicts critical heat fluxes which are on average 7.7% higher than the measured values, however no systematic G-effect can be seen from the plot. Fig. 12 shows the same plot for the data of Table 14. The computed values are on average 8.6% lower than the measured ones. The discrepancy is considerably larger for the data obtained at $G<0.5\times10^6$.

From this comparison we conclude that a difference in F_G of 20% causes an uncertainty in the evaluation of the average value of the critical heat flux of 18%. Our correlation was obtained from data with F_G-values differing less than 7% from 1 and we may infer that this causes an uncertainty of less than 6.1% in the prediction of the critical heat flux, which of course is considerably less than our RMS-error for the data with spacer grids (12.7%).

3.3.5 Effect of changing the range of mass velocity and/or quality

Table III shows two typical cases of APWR. In both the mass velocity is considerably above 10^6 lb/hrft^2 and the local steam quality is strongly negative (large subcooling). The range of validity of the present calculation is down to mass velocities of 0.05×10^6 lb/hrft^2 and up to steam qualities of 0.96 (see Table V), therefore it was felt that it would be worthwhile to investigate the effect of a restriction of the validity range of the mass velocity and steam quality nearer to the interesting application range. Fig. 13 shows the ratio ψ versus G for the spacer grid tests for the data with $G>10^6$ lb/ft^{2}hr only. ϕ_{CHF} has been computed with the standard Q and V values. The present correlation predicts critical heat fluxes which are on average only 2.4% higher than the measured ones. The RMS-error is 11.65% against 12.73% for all the data.

Fig. 14 shows the ratio ψ versus G for the spacer grid tests for the data with $G>10^6$ lb/ft^{2}hr and $X<0.05$ only. Again the computed critical heat fluxes are on average slightly higher than the measured (4.5%). The RMS-error is 11.93%.

In both the cases considered the discrepancies between computed and measured critical heat fluxes appear to be small, in any case much less than the standard deviations. Figures 15 and 16 shows the same data in the plot computed ϕ_{CHF} versus experimental ϕ_{CHF}.

3.3.6 Comparison of computed and experimental ϕ_{CHF}-values at constant pressure, inlet enthalpy and mass velocity

Figures 17 to 23 show the computed critical heat fluxes (lines) and the experimental values (points) versus the inlet enthalpy. Each plot is for a constant pressure, thus constant inlet enthalpy means constant inlet subcooling in this case. Various curves have been plotted for constant values of mass velocity (the values indicated in the plots are for G in 10^6 lb/hr ft^2). For each plot the geometrical parameters and the heat flux distribution are the same. The points compare relatively well with the computed lines.

3.4 Application of the present CHF-correlation to cases typical of the APWR

The present CHF-correlation has been applied to two typical cases of APWR: a homogeneous reactor, and the seed of a heterogeneous reactor. The seed was chosen because there the heat fluxes at the fuel rod surface are higher than in the blanket. The reactor data are from reference |4| and they are shown in Table VI. The axial position chosen, characterized by the distance z in inches from the beginning of the heating region in the core, corresponds to the section where the safety margin to the critical heat flux is a minimum.

The present correlation (equations (26) and (28)) may be applied directly to the case of the seed of a heterogeneous reactor, which has spacer grids very similar to those of the LWBR, however, in the case of the homogeneous reactor with spiral rib spacers (and also in the case of the blanket of the heterogeneous reactor), the present correlation (equations (26) and (30)) cannot be applied directly. Indeed the fuel element clusters of the homogeneous reactor of ref. |4| are not exactly geometrically similar to the cluster tested at Columbia |18|. In particular the axial pitch (H) of the spiral ribs is in the reactor case considerably larger than in the test case (H/d = 50 in the first,

H/d = 13.6 in the second case, where d = rod diameter). Therefore for the application of the present correlation we recommend a correction of the function V of equation (30) to take account of this geometry difference. In this, we make two assumptions:

- that the effect of the spiral ribs on V disappears when the mass velocity tends to zero,
- that the effect of the spiral ribs on V is proportional to the increase in the friction factor of the cluster caused by spiral ribs themselves.

Ref. |19| gives a general correlation for the friction factor of rod clusters with spiral spacers. According to this general correlation and the two above mentioned assumptions, equation (30) is modified as follows:

$$V = 1 - 0.2589 \frac{F^{0.915}}{(D_h\,|m|)^{0.17}} \left[0.25 + 0.1\,G + 2.75 \exp(-4G) - 3 \exp(-3\,G) \right] \qquad (32)$$

where

$$F = \left(\frac{P}{d}\right)^{0.5} + \left[7.6 \frac{(P/d)^3}{H/d} \right]^{2.16}$$

P = pitch of the rods in the cluster
d = rod diameter
H = axial pitch of the spiral spacer ribs
$D_h|m|$ = hydraulic diameter of the coolant channel in meters.

Table VI shows the results of the application of the present correlation to the two chosen typical APWR cores. In the case of the seed of the heterogeneous reactor (relatively large coolant channel, spacer grid) our prediction is very near to that of the Shippingport correlation |5| (see Table III). This is not surprising since, for the clusters with grid spacers, the two correlations are based on the same experimental evidence (or, as stated in the Light Water Breeder Reactor Safety Report |6|, the Shippingport correlation has been qualified by the same experiments). However, the critical heat flux predicted by our correlation is considerably higher than that of the WSC-2 (+14%) and of the B&W-VPI&SU (+39%) correlations, and of course much smaller than those of the correlations developed for PWR's (see Table III).

In the case of the homogeneous reactor, due to the very small coolant channel hydraulic diameter, our prediction is much smaller not only of the PWR correlations but of the Shippingport prediction as well (see Table III). Again our prediction is considerably higher than that of the WSC-2 (+50%, but the WSC-2 correlation was not developed for D_h values as low as 0.1045 in) and of the B&W-VPI&SU (+28%) correlations. This is probably due, at least in part, to the fact that we take account of the spiral spacer effect by means of the Columbia tests.

4. Concluding remarks

The geometry dependent parameters of the WSC-2 correlation were determined again from the experimental data obtained at the Bettis Laboratory in the frame of the Light Water Breeder Reactor Programme and from experiments performed at the Columbia University. In this, due account was taken of the difference in hydraulic diameter of the outer coolant channels near the cluster wall and of the non-uniform radial distribution of the heat flux. The new values for a triangular array rod cluster are:

$$Q_1 = 1.763, \qquad Q_2 = 9.157, \qquad Q_4 = 6.507$$

and

$$V = 3.1 - 1.15\,G + 0.1188\,G^2 - 2.5\exp(-G) \quad \text{clusters with grid spacers}$$

$$V = 1 - \left[0.25 + 0.1\,G + 2.75\exp(-4G) - 3\exp(-3G)\right] \quad \text{clusters with spiral rib spacers.}$$

The RMS-error was 12.7% for the 695 data points with grid spacers and 6.2% for the 44 data points with spiral rib spacers.

The validity range of the present correlation is determined by the experimental evidence on which the correlation is based and it is given in Table V. Essentially we have extended the WSC-2 correlation to smaller coolant channels of clusters of rods (D_h = 0.09 in instead of 0.2 in) and more negative local steam qualities (X = -0.45 instead of -0.2). These extended ranges are relevant for the APWR. Furthermore the spacer parameter V has been determined in more detail (in the WSC-2 correlation it is assumed as a constant).

For reactor application in the case of spiral ribs the function V has been corrected to take account of the fact that the fuel element clusters are not always geometrically similar to the cluster tested at Columbia, whose results were used for the present correlation. The correction factor has been assumed proportional to the increase in the friction coefficient of the cluster caused by the spiral ribs.

The critical heat fluxes predicted with the present correlation are much smaller than those calculated with the usual PWR-CHF correlations. This may be due to the fact that the flow instabilities due to the formation of steam bubbles in the parallel coolant channels of the rod clusters are more pronounced in the case of coolant channels with smaller hydraulic diameters. However the predictions of the present correlation lie considerably above those of the WSC-2 and B&W-VPI&SU correlations. This is probably due to the fact that we consider the effect of the mass velocity on the spacer parameter V.

It is clear that before building an APWR it is necessary to perform out-of-pile critical heat flux tests with the proper geometrical and thermohydraulic conditions of the most rated fuel element. For the time being however the present correlation appears to be good enough for parametric and optimisation studies.

References

/1/ Hennies, H., and Märkl, M.:
Überlegungen zur Modifizierbarkeit eines LWR im Hinblick auf eine bessere Uranausnutzung; Jahrestagung Kerntechnik, Berlin, 25.-27. März 1980

/2/ Rau, P. et al.:
Ergebnisse der Vorstudie für einen Leichtwasserreaktor mit besserer Uranausnutzung, Jahrestagung Kerntechnik, Berlin, 25.-27. März 1980

/3/ Jansen, P., Hennies, H., and Klumpp, P.:
Uran- und Plutoniumverfügbarkeit für Leichtwasserreaktoren, Hochkonverter und Schneller Brüter, Fachtagung: Neuere Entwicklungen in der Reaktortechnik, Bonn, 27.-28. Oktober 1980

/4/ Dalle Donne, M.:
Fluid- und thermodynamic calculations for an advanced pressurized light water reactor with a tight fuel rod lattice; Jahrestagung Kerntechnik, Düsseldorf, 24.-26. März 1981

/5/ Westinghouse Electric Corporation, Bettis Atomic Power Laboratory
Pressurized Water Reactor Project Technical Progress Report, April-June 1961, USAEC Report WAPD-MRP-92.

/6/ Light Water Breeder Reactor Safety Report, unpublished

/7/ Tong, L.S.:
An evaluation of the departure from nucleate boiling in bundles of reactor fuel rods, Nuclear Science and Engineering, 33, 7-15, 1968

/8/ Gellerstedt, J.S. et al:
Correlation of critical heat flux in a bundle cooled by pressurized water, Symposium on Two Phase Flow and Heat Transfer in Rod Bundles, ASME Winter Meeting, Los Angeles, Calif., 1969

/9/ Lawrence, F.D. et al.:
Critical heat flux in PWR fuel assemblies, AIChe-ASME Heat Transfer Conf., Salt Lake City, August 1977

/10/ Bowring, R.W.:
WSC-2, a subchannel dryout correlation for water-cooled clusters over the pressure range 3.4-15.9 MPa, AEEW-R983, 1979

/11/ Edlund, M.C. et al.:
Technical feasibility of a pressurized water reactor design with a low water volume fraction lattice, EPRI-NP-1833, May 1981

/12/ Green, S.J. et al:
Critical heat flux tests on a coolant channel simulating a closely spaced lattice of rods, WAPD-TM-466, Bettis Atomic Power Laboratory, Pittsburgh, Pa., 1969, see also in Symposium on Two-Phase Flow and Heat Transfer in Rod Bundles, ASME Winter Meeting, Los Angeles, Calif., 1969

/13/ LeTourneau, B.W. et al.:
Critical heat flux and pressure drop tests with parallel upflow of high pressure water in bundles of twenty 0.25 and 0.28 in diameter rods, WAPD-TM-1013, 1975

/14/ Rosal, E.R. et al.:
High pressure rod bundle DNB data with axially non-uniform heat flux, Nucl. Engr. & Design, 31, 1-20, 1974

/15/ LeTourneau, B.W. et al.:
Critical heat flux and pressure drop tests with parallel upflow of high pressure water in bundles of twenty 3/4 in rods. Nucl. Sci.Eng., 54, 214-232, 1974

/16/ Coeling, K.J.:
Critical heat flux and pressure drop tests with vertical upflow of water in a 20-rod bundle of 0.695 in diameter rods, WAPD-TM-1155, 1977

/17/ Tong, L.S.:
Critical heat fluxes in rod bundles, in "Two phase flow and heat transfer in rod bundles", ed. V.E. Schrock, p. 31, ASME, New York, 1969

/18/ Hatzner, B.:
Heat transfer and hydraulic studies for SNAP-4 fuel element geometries Columbia University, Engineering Research Laboratories, Sept. 1963, TID 19563.

/19/ Rehme, K.:
Systematische experimentelle Untersuchungen der Abhängigkeit des Druckverlustes von der geometrischen Anordnung für längsdurchströmte Stabbündel mit Spiralabstandshaltern, Ext. Bericht INR-4/68-16, Kernforschungszentrum Karlsruhe, Februar 1968.

APPENDIX I: Conversion factors

G:	10^6 lb/hr ft^2 = 1356 kg/m^{2}sec
D_h, z:	1 in. = 0.0254 m
p:	1 p.s.i.a. = 0.06893 bar
$\Delta h, \lambda$:	1 BTu/lb = 2325 J/kg
ϕ:	10^6 Btu/ft^2 hr = 3155 kW/m^2

Table I: CHF Correlations from the Literature

Correlation name	Year	Reference	Range of Application			
			p(p.s.i.a)	$Gx10^{-6}$ (lb/hr ft^2)	D_h(in)	X_{local}
Shippingport	1961	/5/	?	?	0.2	?
W-3	1968	/7/	1000÷2300	1 ÷5	0.2 ÷0.7	-0.15÷0.15
B&W-2	1969	/8/	2000÷2400	0.75÷4.0	0.2 ÷0.5	-0.03÷0.2
Combustion Eng.	1977	/9/	1785÷2415	0.9 ÷3.2	0.36÷0.54	-0.16÷0.2
WSC-2	1979	/10/	435÷2400	0.2 ÷3.7	0.2 ÷1.2	-0.2 ÷0.86
B&W-VPI&SU	1981	/11/	1200÷2425	1 ÷4.2	0.14÷0.85	inlet sub-cooling 30÷440 ^{o}F

Table II: Experimental Data Base for B&W-VPI&SU CHF-Correlation

Data Source |Reference|	p(p.s.i.a.)	$Gx10^{-6}$ (lb/hr ft^2)	D_h(in)	Inlet sub-cooling (^{o}F)	No.of points used
|12|	1200÷2000	1.0÷4.2	0.142÷0.152	40÷440	53
|13|	1200÷2000	1.0÷4.0	0.175÷0.260	30÷400	148
|14|	1500÷2425	2.0÷3.6	0.85	30÷140	47
Composite	1200÷2425	1.0÷4.2	0.142÷0.85	30÷440	248

Table III: Application of the CHF-Correlations from the Literature to two Typical Cases of the APWR |4|.

Correlation denomination	Correlation prediction: $\phi \cdot 10^{-6}$ |Bt /hr ft^2|	
	Homogeneous reactor	Heterogenous reactor (seed)
Shippingport |5|	1.351	0.823
W-3 |7|	4.901	1.858
B&W-2 |8|	2.193	1.383
Combustion Eng. |9|	2.201	1.280
WSC-2 |10|	0.565	0.735
B&W-VPI&SU |11|	0.660	0.604

For the homogeneous reactor case:

$p = 2320$ p.s.i.a., $G = 4.6 \times 10^6$ lb/hr ft^2,

$D_h = 0.1045$ in, $X = -0.32$, $z = 39.96$ in

For the heteregeneous (seed) reactor case:

$p = 2310$ p.s.i.a., $G = 3.92 \times 10^6$ lb/hr ft^2,

$D_h = 0.2166$ in, $X = -0.1007$, $z = 57.76$ in.

Table IV: WSC-2 correlation

$$\phi(x10^6 \text{ Btu/hr ft}^2) = \frac{A+B\Delta H_i}{C+ZY}$$

$$A = \frac{0.25\ GD\lambda F_1 Q_1}{1+Q_2 F_2 GD} \qquad B = 0.25GD$$

$$C' = \frac{Q_4 F_3 \sqrt{GD}}{D_h} \qquad C = C'V\left[1 + \frac{Y-1}{1+G}\right]$$

where: $D=F_p D_h$; D_h=coolant channel hydraulic diameter (in)

F_p= radial form factor in the considered section of the bundle

$p_r=10^{-3}p$ p=pressure (p.s.i.a.)

$F_1=p_r^{0.982}e^{1.17(1-p_r)}$

$F_2=p_r^{0.841}e^{1.424(1-p_r)}$

$F_3=p_r^{1.851}e^{1.241(1-p_r)}$

G = mass velocity (10^6 lb/ft^2 hr)

λ = latent heat of evaporation (Btu/lb)

ΔH_i=inlet subcooling (Btu/lb)

z = distance from channel inlet (in)

y = ratio of average cluster heat flux from entry to z
to local cluster radial-average heat flux at z

V = grid spacers parameter. For the best fit of experimental data V = 0.7.

geometry parameter	Q_1	Q_2	Q_4
triangular array	1.329	2.372	12.26

Data Source |Reference|	Table No. in present Work	Spacer type	Number of Rods	Rod Diameter |in|	Pitch to Diameter Ratios	Rod Heated Length |in|	Infinite Array Hydraulic Diameter |in|	Transversal Heat Flux Distribution	p |p.s.i.a.|	$G \times 10^{-6}$ |lb/hr ft^2|	X Average exit Quality	No. of Data points
|15|	1.1	grid	20	0.75	1.02	94	0.110	1.5 : 1	1200÷2000	0.255÷3.05	-0.12÷0.64	48
	2.1		20	0.75	1.02	94	0.110	uniform	1200÷2000	0.254÷3.02	0.14÷0.85	51
|13|	3.1+3.2	grid	20	0.25	1.36	54	0.260	1.5 : 1	1200÷2000	0.247÷4.03	-0.42÷0.51	71
	4.1+4.2			0.25	1.36	54	0.260	1.5 : 1	1200÷2000	0.229÷4.02	-0.45÷0.50	78
	5.1+5.2			0.25	1.36	54	0.260	uniform	1200÷2000	0.248÷3.62	-0.44÷0.69	75
	6.1			0.25	1.36	54	0.260	1.5 : 1	1200÷2000	0.248÷3.88	-0.30÷0.47	50
	7.1			0.25	1.36	54	0.260	1.5 : 1	1195÷2010	0.284÷3.46	-0.40÷0.42	55
	8.1			0.25	1.36	54	0.260	uniform	1195÷2008	0.232÷2.00	-0.01÷0.69	25
	9.1			0.25	1.36	54	0.260	uniform	1200÷2000	0.247÷2.01	-0.34÷0.64	33
	10.1			0.25	1.36	33	0.260	uniform	1200÷2000	0.249÷3.00	-0.11÷0.48	26
	11.1			0.28	1.21	54	0.175	uniform	1200÷2000	0.248÷4.00	-0.17÷0.75	45
	12.1+12.2			0.28	1.21	54	0.175	uniform	400÷2000	0.05 ÷3.03	-0.02÷0.96	70
|16|	13.1+13.2	grid	20	0.695	1.10	94	0.234	1.37: 1	1200÷2000	0.10 ÷2.02	-0.28÷0.90	68
|18|	15.1	spiral ribs	12	0.44	1.051	17	0.0903	uniform	1200	0.48 ÷4.09	-0.02÷0.53	44
composite				$\frac{0.25}{0.75}$	$\frac{1.02}{1.36}$	$\frac{17}{96}$	$\frac{0.09}{0.26}$		400÷2010	0.05 ÷4.09	-0.45÷0.96	739

Table V: Experimental Data Base for the Present CHF-Correlation

Table VI: Application of the present CHF-correlation to two typical cases of the APWR |4|

Correlation	Correlation prediction: $\phi_{CHF} \times 10^{-6}$ |Btu/hr ft^2|	
	Homogeneous Reactor	Heterogeneous Reactor (seed)
WSC-2 |10|	0.565	0.735
B&W-VPI&SU |11|	0.660	0.604
Present correlation	0.849 Eqs. (26),(32)	0.838 Eqs. (26),(28)

For the homogeneous reactor case:

$p = 2320$ p.s.i.a.,
$G = 4.6 \times 10^6$ lb/hr ft^2,
$D_h = 0.1045$ in,
$X = -0.31$, $z = 39.96$ in

For the heterogeneous (seed) reactor case:

$p = 2320$ p.s.i.a.,
$G = 3.92 \times 10^6$ lb/Hr ft^2,
$D_h = 0.2166$ in,
$X = -0.1007$, $z = 57.76$ in

Tables : 1, 2, 3, 4, 5, 6, 7, 8, 9, 10 11, 12, 13

Q_1 = 1.763 $\quad\quad$ $\bar{e}$ = -1.97 %

Q_2 = 9.157 $\quad\quad$ σ = 13.75 %

Q_4 = 9.295 $\quad\quad$ ε_{RMS} = 13.89 %

V=0.700

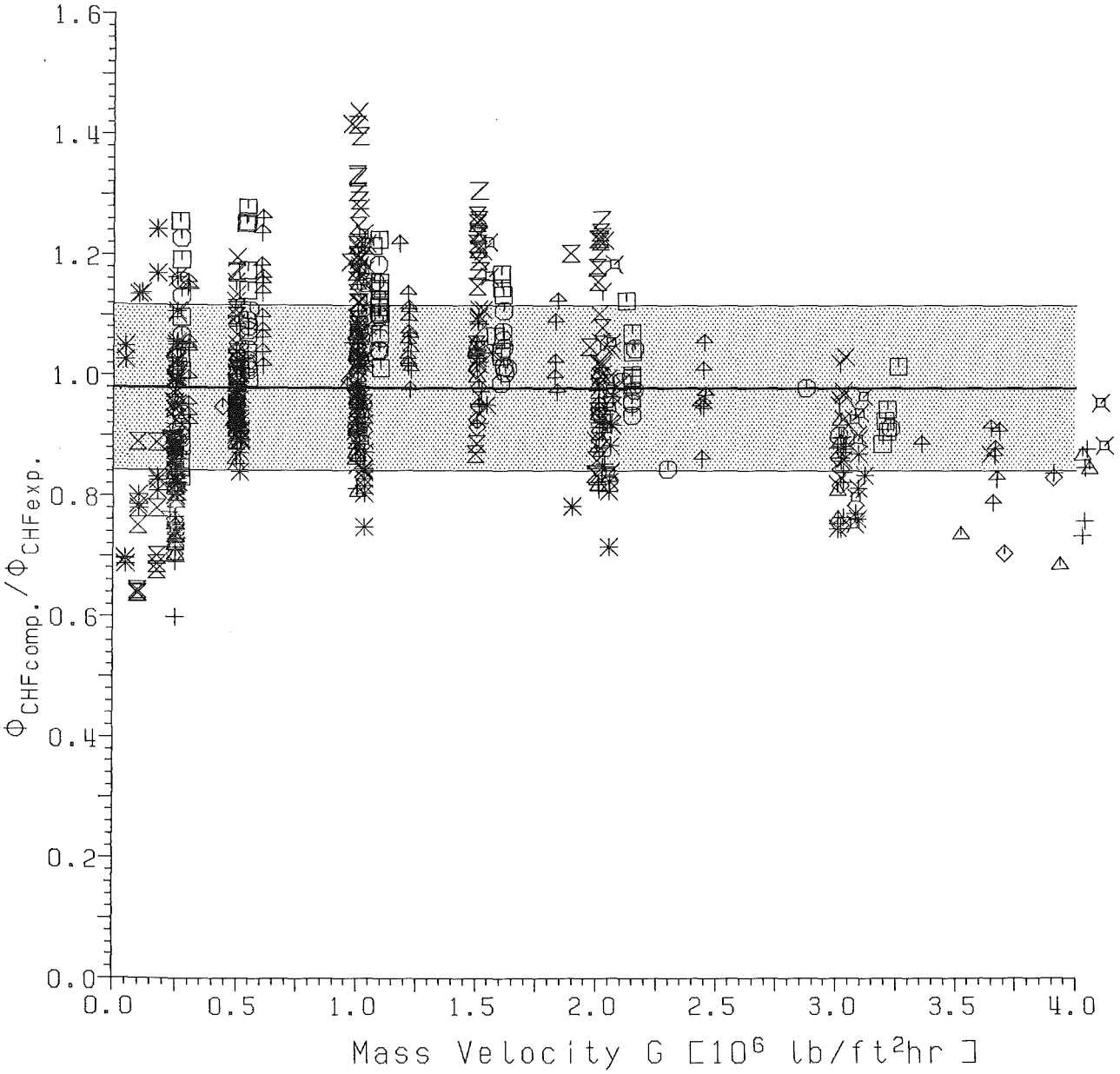

Fig.1 Spacer grid data (Tables 1-13). φ vs. G for V=0.7.

Experimental Data

Tables	:	1,2,3,4,5,6,7,8,9,10,11,12,13
Number of data points	:	695
		$\nu = 0.7$

Geometry dependent constants

Q1	:	1.763
Q2	:	9.157
Q4	:	9.259

Results

Mean error	:	-1.97 %
Standard deviation	:	13.75 %
RMS-error	:	13.89 %
lower limit	:	-40.08 %
upper limit	:	43.80 %

Comments to Fig. 1.

Tables : 1, 2, 3, 4, 5, 6, 7, 8, 9, 10 11, 12, 13

Q_1 = 1.763 $\bar{e}$ = -1.97 %

Q_2 = 9.157 σ = 13.75 %

Q_4 = 6.507 ε_{RMS} = 13.89 %

V=1.000

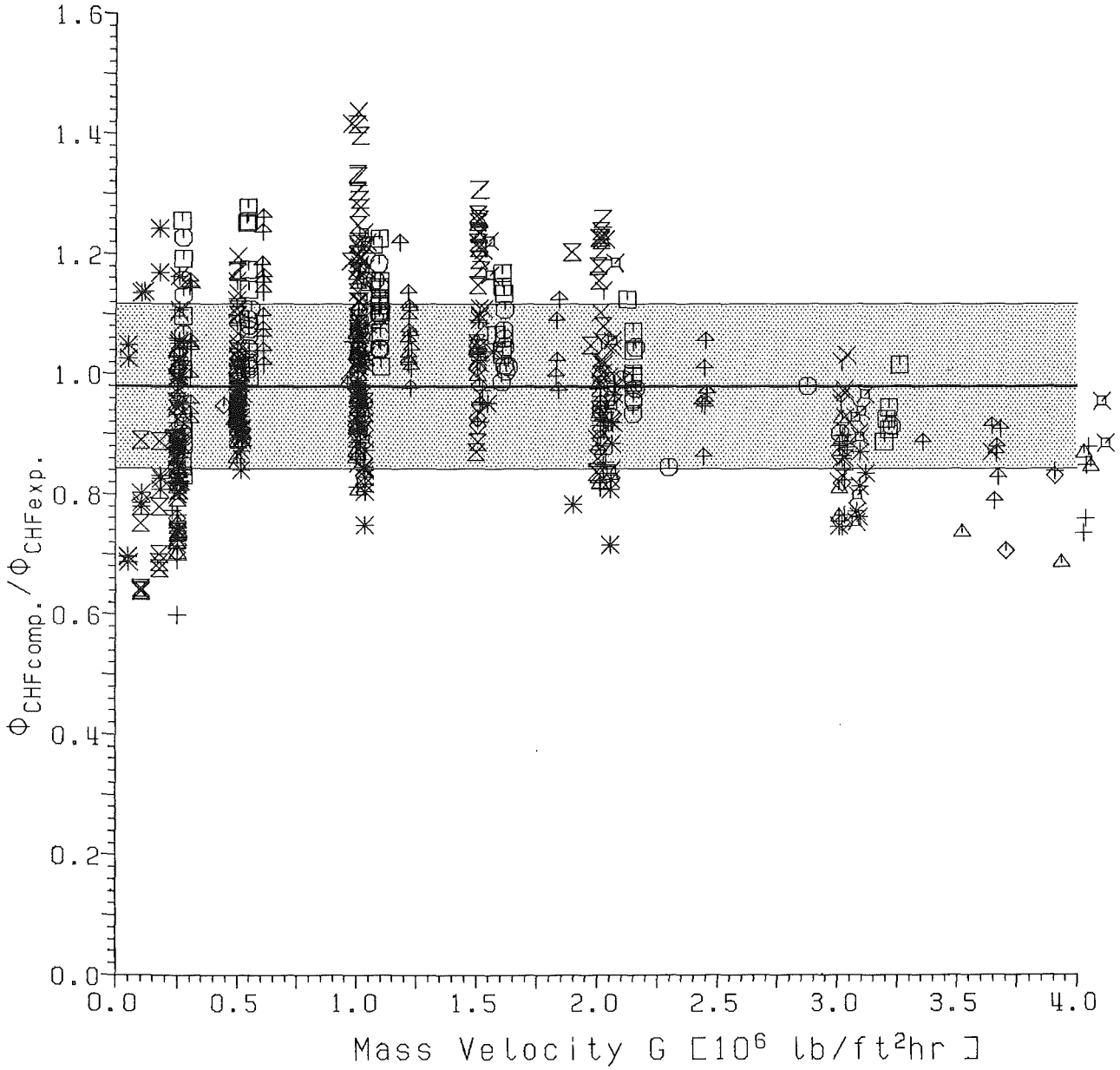

Fig.2 Spacer grid data (Tables 1-13). ϕ vs. G for V=1.

Experimental Data

Tables	:	1,2,3,4,5,6,7,8,9,10,11,12,13
Number of data points	:	695
		v = 1.0

Geometry dependent constants

Q1	:	1.763
Q2	:	9.157
Q4	:	6.507

Results

Mean error	:	-1.97 %
Standard deviation	:	13.75 %
RMS-error	:	13.89 %
lower limit	:	-40.08 %
upper limit	:	43.80 %

Comments to Fig. 2.

Tables : 1, 2, 3, 4, 5, 6, 7, 8, 9, 10 11, 12, 13

$Q_1 = 1.763$

$Q_2 = 9.157$

$Q_4 = 6.507$

$V = 3.1-1.15*G+0.1188*G^2-2.5*\exp(-G)$

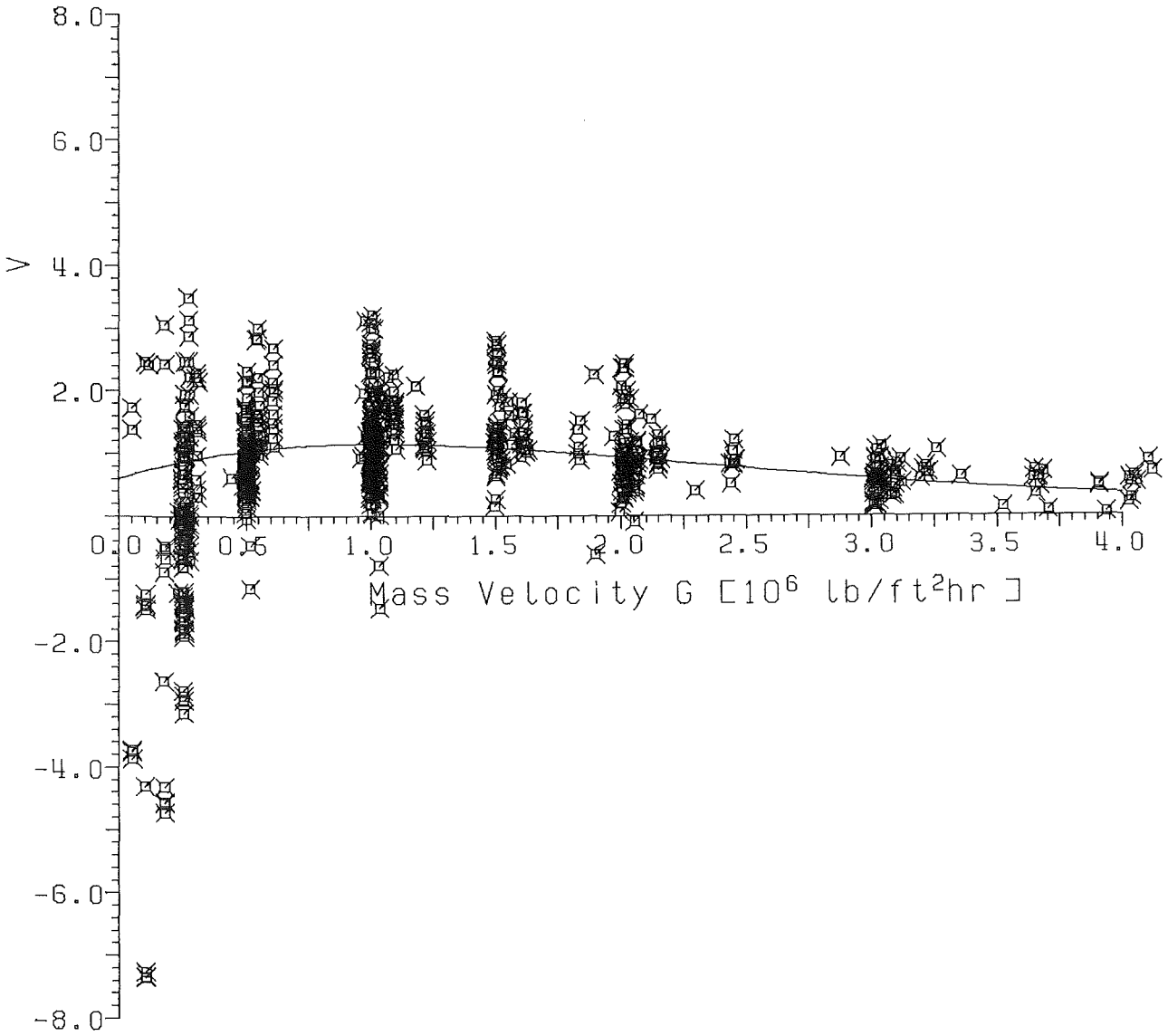

Fig.3 Spacer grid data (Tables 1-13). V vs. G for standard Q-values and $\Phi_{CHF}=\Phi_{CHFexp.}$

Tables : 1, 2, 3, 4, 5, 6, 7, 8, 9, 10 11, 12, 13

$Q_1 = 1.763$ $\quad \bar{e} = -0.79\ \%$

$Q_2 = 9.157$ $\quad \sigma = 12.71\ \%$

$Q_4 = 6.507$ $\quad \varepsilon_{RMS} = 12.73\ \%$

$V = 3.1-1.15*G+0.1188*G^2-2.5*\exp(-G)$

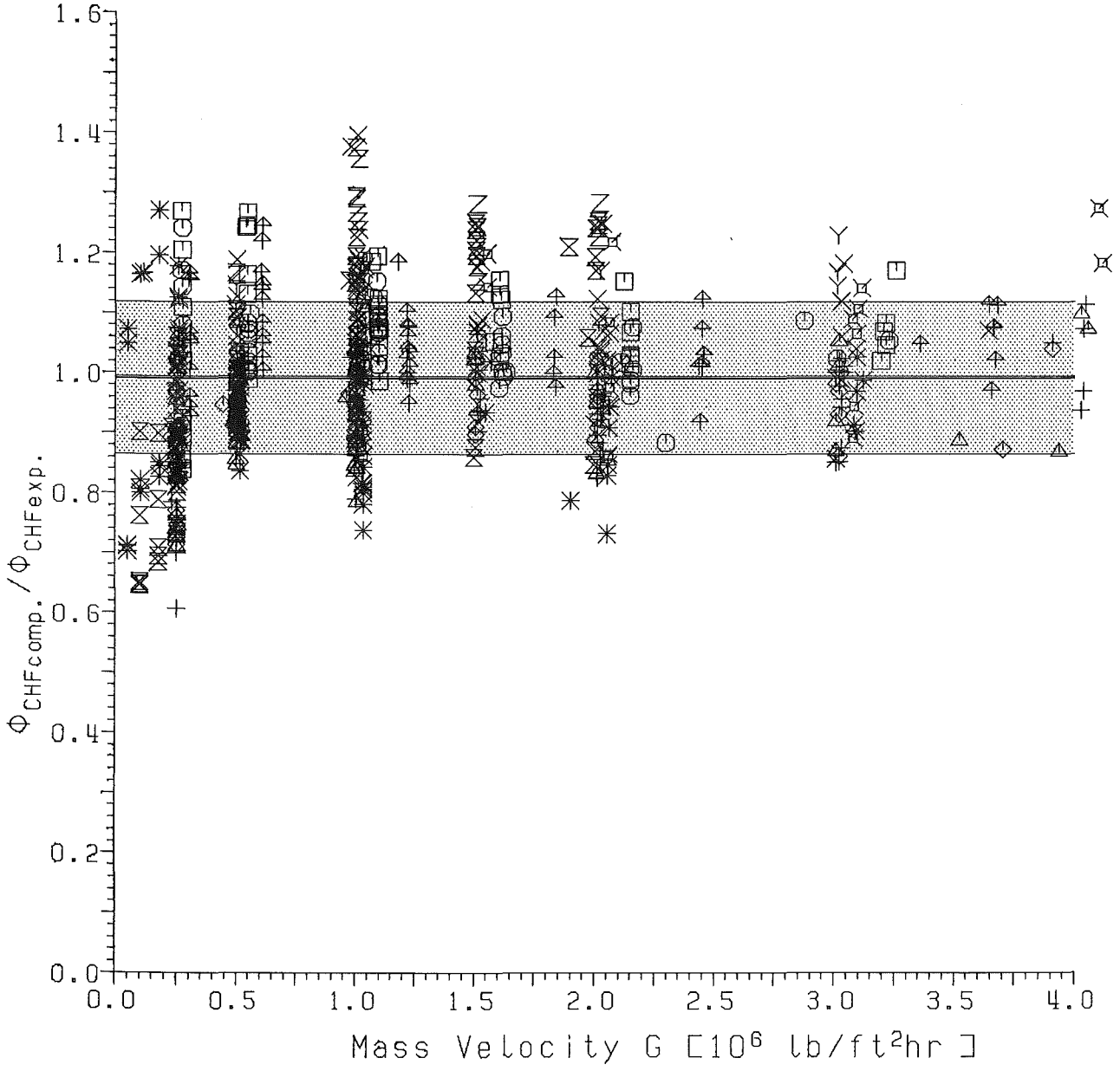

Fig.4 Spacer grid data (Tables 1-13). φ vs. G for standard Q-values and optimum V=V(G) function.

Experimental Data

Tables	:	1,2,3,4,5,6,7,8,9,10,11,12,13
Number of data points	:	695

optimum function V(G) = 3.1-(1.15-0.1188*G)*G-2.5*exp(-G)

Geometry dependent constants

Q1	:	1.763
Q2	:	9.157
Q4	:	6.507

Results

Mean error	:	-0.79	%
Standard deviation	:	12.71	%
RMS-error	:	12.73	%
lower limit	:	-39.27	%
upper limit	:	39.65	%

Comments to Fig. 4.

Tables : 1, 2, 3, 4, 5, 6, 7, 8, 9, 10 11, 12, 13

$Q_1 = 1.763$ $\quad \bar{e} = -0.79\ \%$

$Q_2 = 9.157$ $\quad \sigma = 12.71\ \%$

$Q_4 = 6.507$ $\quad \varepsilon_{RMS} = 12.73\ \%$

$V = 3.1-1.15*G+0.1188*G^2+2.5*\exp(-G)$

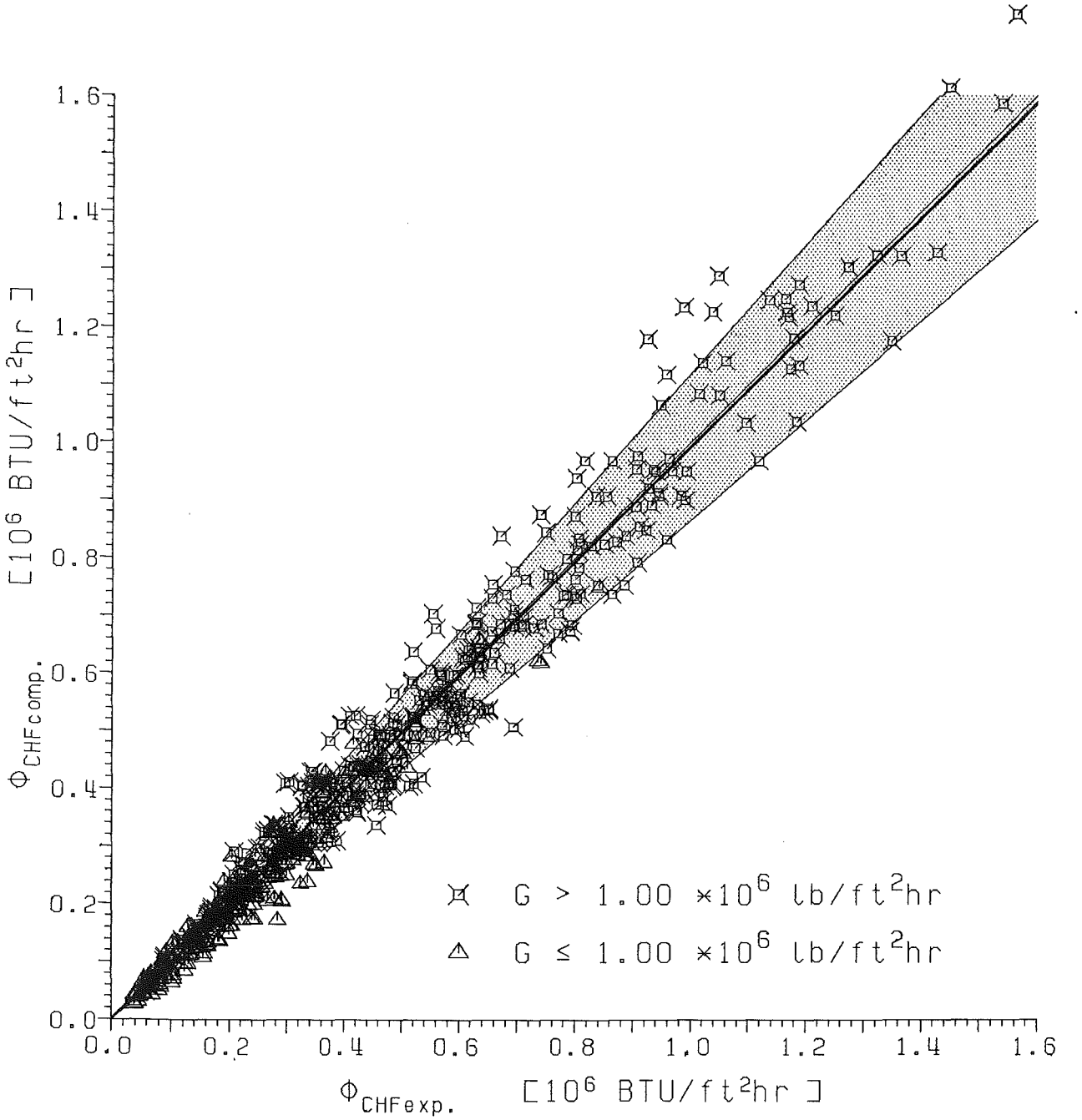

Fig.5 Spacer grid data (Tables 1-13). $\Phi_{CHFcomp.}$ vs. $\Phi_{CHFexp.}$ for standard Q-Values and optimum V=V(G) function.

Tables : 1, 2, 3, 4, 5, 6, 7, 8, 9, 10 11, 12, 13

$Q_1 = 1.763$ $\quad \bar{\varepsilon} = -0.79\ \%$

$Q_2 = 9.157$ $\quad \sigma = 12.71\ \%$

$Q_4 = 6.507$ $\quad \varepsilon_{RMS} = 12.73\ \%$

$V = 3.1-1.15*G+0.1188*G^2-2.5*\exp(-G)$

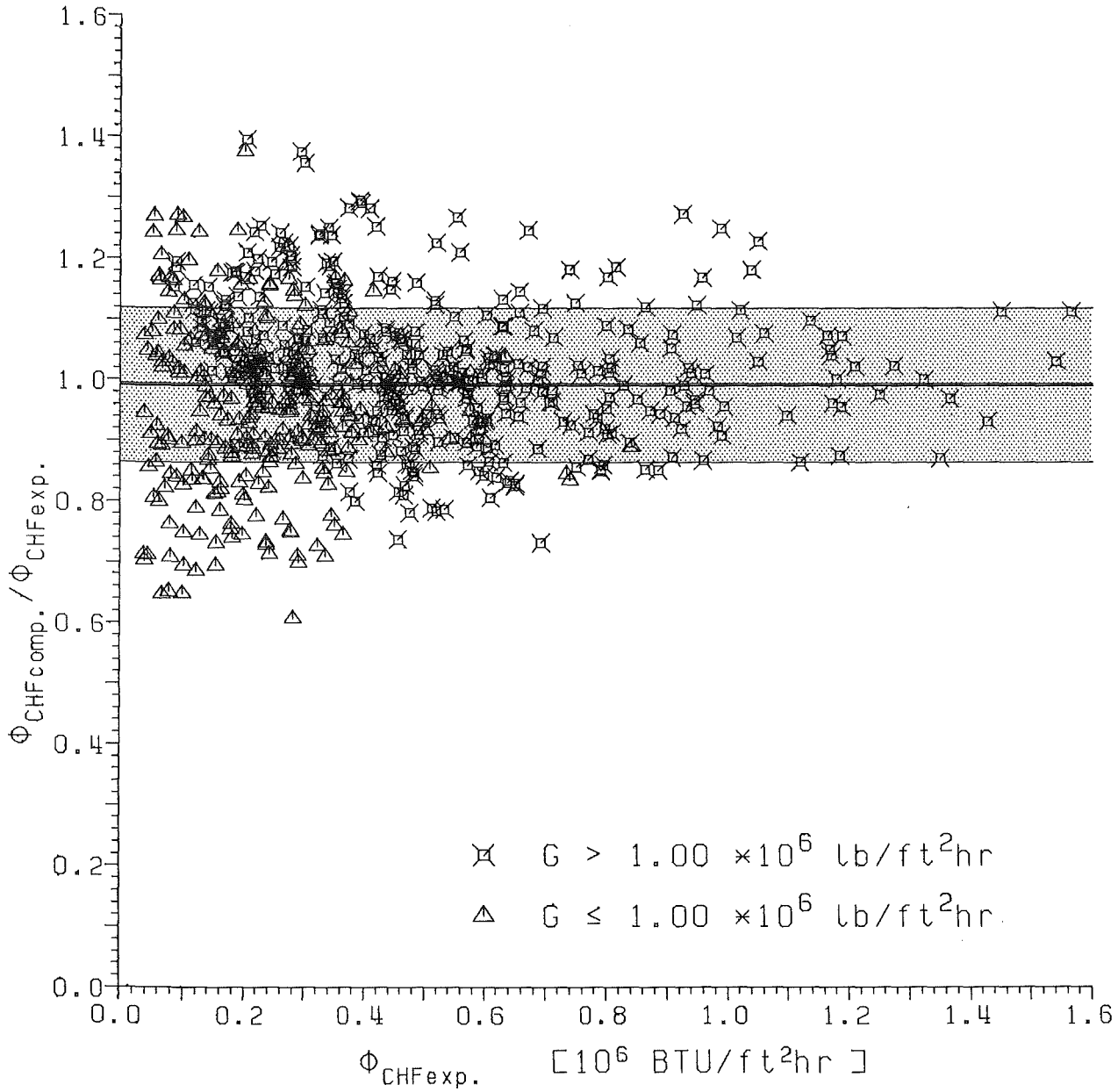

Fig.6 Spacer grid data (Tables 1-13). φ vs. $\Phi_{CHFexp.}$ for standard Q-values and optimum V=V(G) function.

Table : 15

Ⓘ

Q_1 = 1.763 $\bar{e}$ = -29.34%

Q_2 = 9.157 σ = 17.00 %

Q_4 = 6.507 ε_{RMS} = 33.91 %

V=1.000

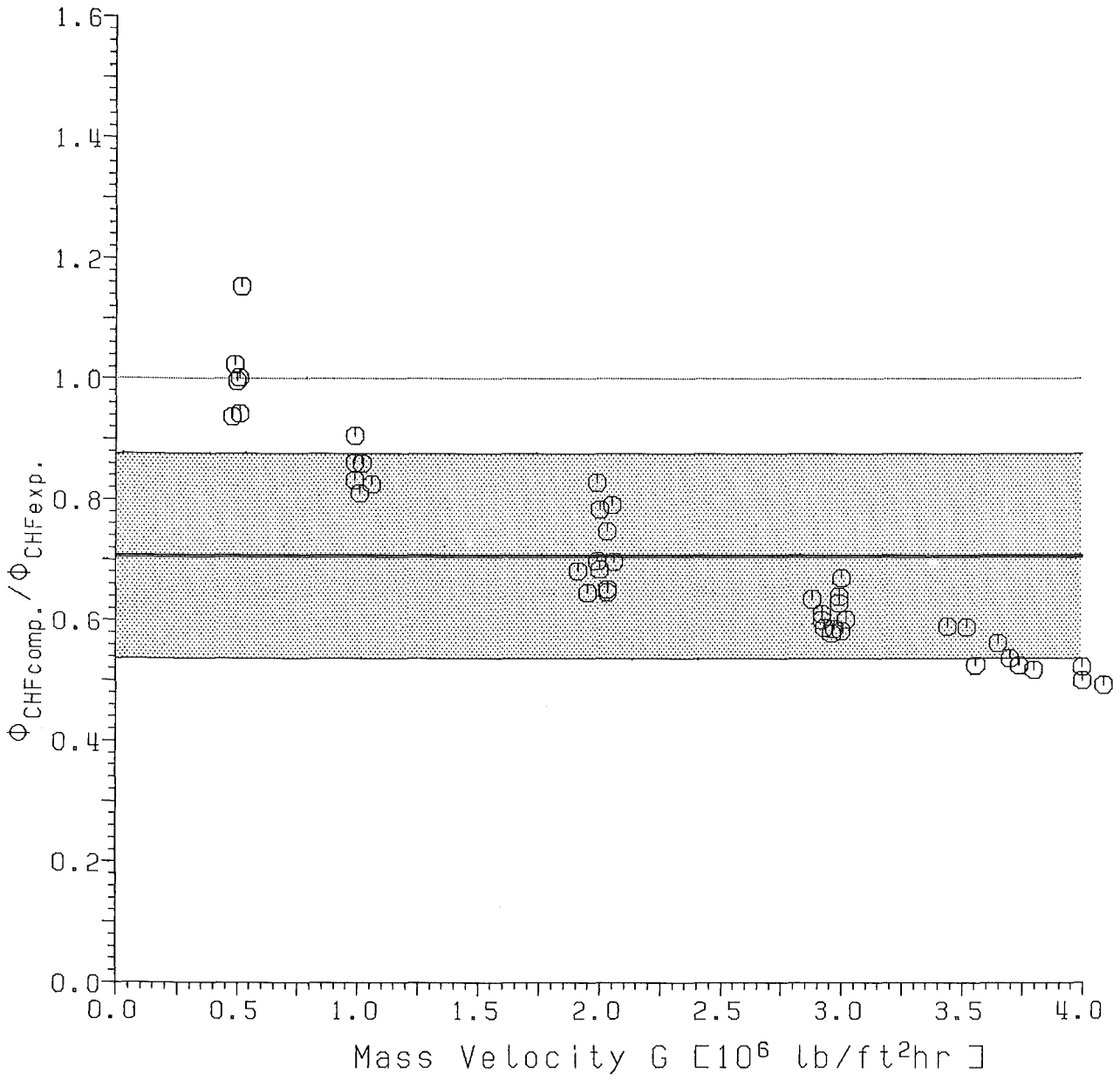

Fig.7 Spiral rib spacer data (Table 15) ϕ vs. G for standard Q-values and V=1.

Experimental Data

Table	:	15
Number of data points	:	44

v = 1.0

Geometry dependent constants

Q1	:	1.763
Q2	:	9.157
Q4	:	6.507

Results

Mean error	:	-29.34	%
Standard deviation	:	17.00	%
RMS-error	:	33.91	%
lower limit	:	-50.71	%
upper limit	:	15.31	%

Comments to Fig. 7.

Table : 15

$Q_1 = 1.763$

$Q_2 = 9.157$

$Q_4 = 6.507$

$V = 1-(.25+0.1*G+2.75*\exp(-4*G)-3*\exp(-3*G))$

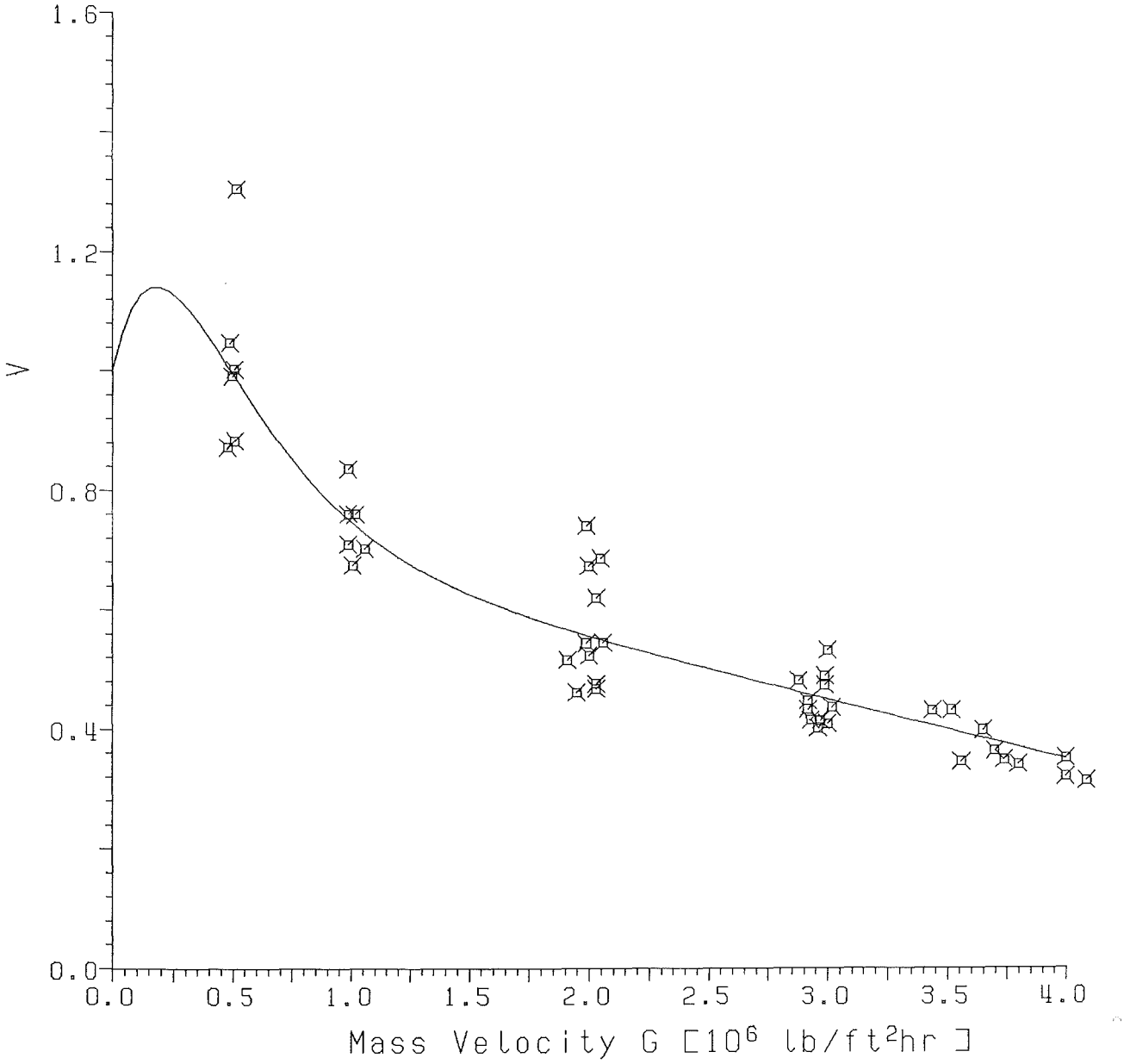

Fig.8 Spiral rib spacer data (Table 15) V vs. G for standard Q-values and $\Phi_{CHF}=\Phi_{CHFexp.}$

Table : 15

Q_1 = 1.763 $\quad \bar{e}$ = -0.07 %

Q_2 = 9.157 $\quad \sigma$ = 6.18 %

Q_4 = 6.507 $\quad \varepsilon_{RMS}$ = 6.18 %

V = 1-(025+0.1*G+2.75*exP(-4*G)-3*exp(-3*G))

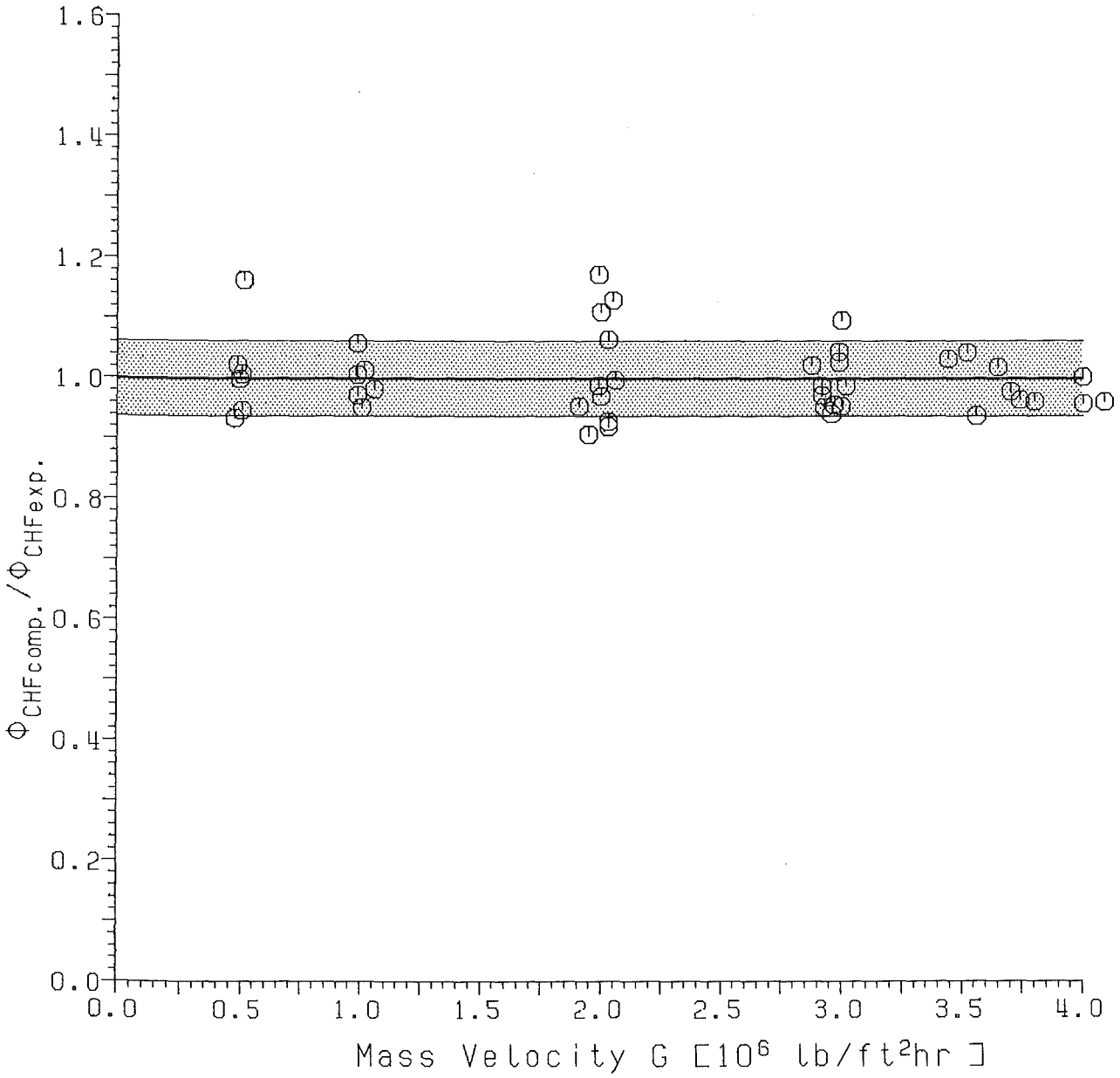

Fig.9 Spiral rib spacer data (Table 15) φ vs. G for standard Q-values and optimum V=V(G) function.

Experimental Data

Table	:	15
Number of data points	:	44

optimum function v(g) = 1-(0.25+0.1*g+2.75*exp(-4*g)-3*exp(-3*g))

Geometry dependent constants

Q1	:	1.763
Q2	:	9.157
Q4	:	6.507

Results

Mean error	:	-0.07	%
Standard deviation	:	6.18	%
RMS-error	:	6.18	%
lower limit	:	-9.33	%
upper limit	:	17.18	%

Comments to Fig. 9.

Table : 15

Q_1 = 1.763 $\quad\quad$ $\bar{e}$ = -0.07 %

Q_2 = 9.157 $\quad\quad$ σ = 6.18 %

Q_4 = 6.507 $\quad\quad$ ε_{RMS} = 6.18 %

$V = 1-(025+0.1*G+2.75*exP(-4*G)-3*exp(-3*G))$

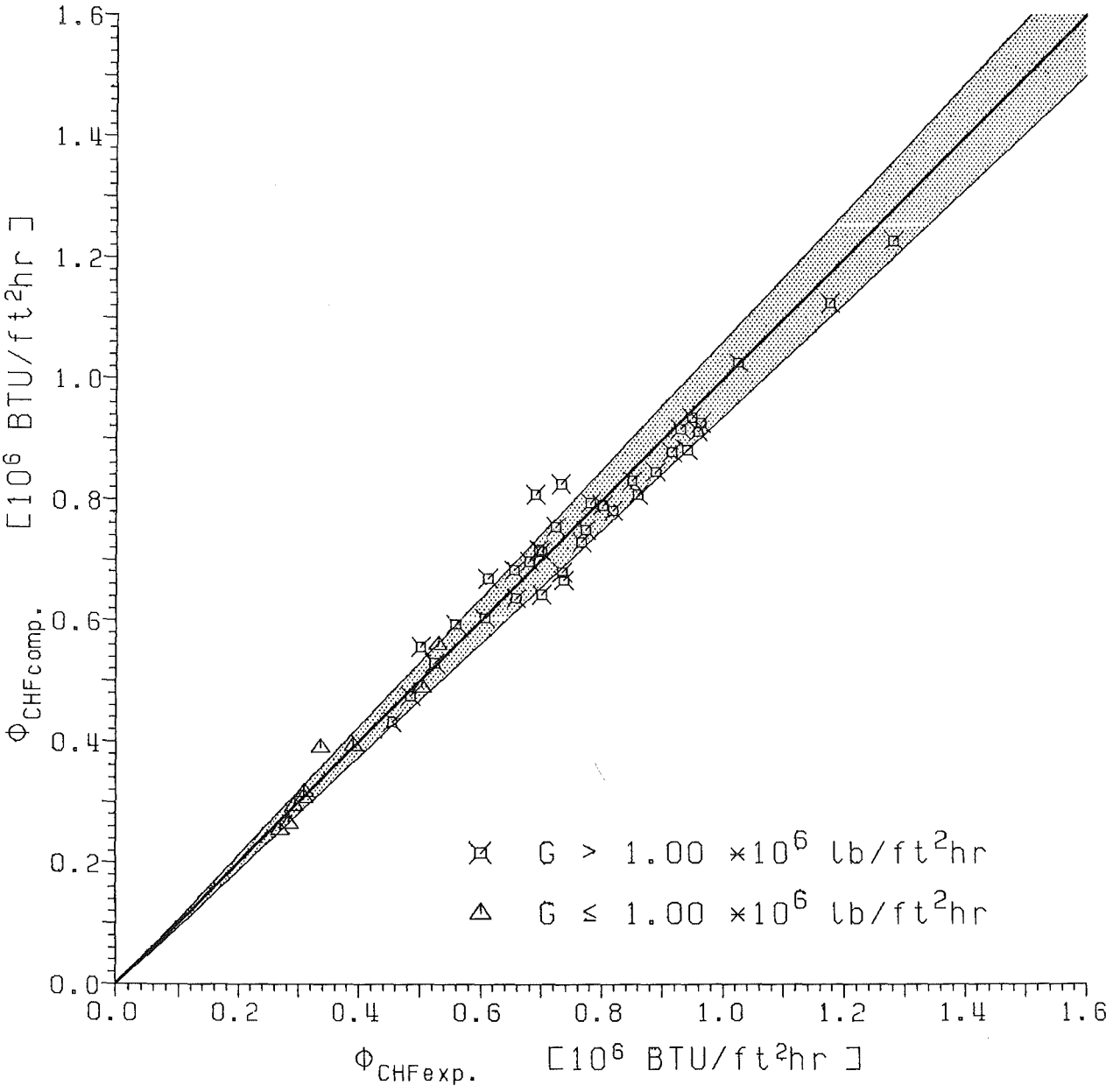

Fig.10 Spiral rib spacer data (Table 15) $\Phi_{CHFcomp.}$ vs. $\Phi_{CHFexp.}$ for standard Q-values and optimum V=V(G) function.

Table : 1

Q_1 = 1.763 $\bar{e}$ = 7.73 %

Q_2 = 9.157 σ = 9.87 %

Q_4 = 6.507 ε_{RMS} = 12.54 %

$V = 3.1-1.15*G+0.1188*G^2+2.5*\exp(-G)$

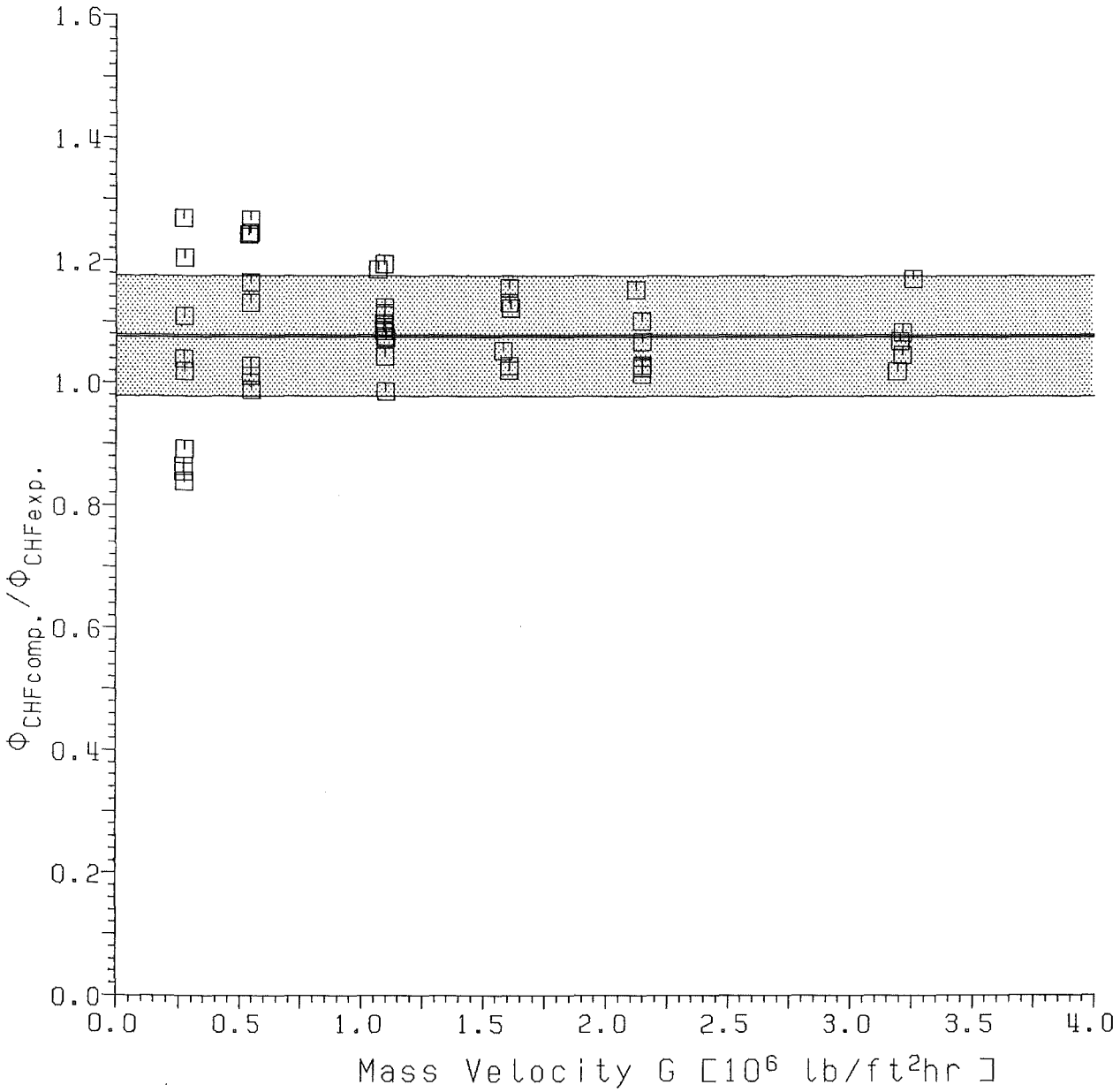

Fig.11 Spacer grid data (Table 1, F_G=1.06855) φ vs. G for standard Q-values and optimum V=V(G) function.

Experimental Data

Table	:	1
Number of data points	:	48

optimum function $v(g) = 3.1-(1.15-.1188*g)*g-2.5*\exp(-g)$

Geometry dependent constants

Q1	:	1.763
Q2	:	9.157
Q4	:	6.507

Results

Mean error	:	7.73	%
Standard deviation	:	9.87	%
RMS-error	:	12.54	%
lower limit	:	-16.01	%
upper limit	:	26.92	%

Comments to Fig. 11.

Table : 14

Q_1 = 1.763 $\quad\quad$ $\bar{e}$ = -8.57 %

Q_2 = 9.157 $\quad\quad$ σ = 13.41 %

Q_4 = 6.507 $\quad\quad$ ε_{RMS} = 15.91 %

$V = 3.1-1.15\times G+0.1188\times G^2-2.5\times \exp(-G)$

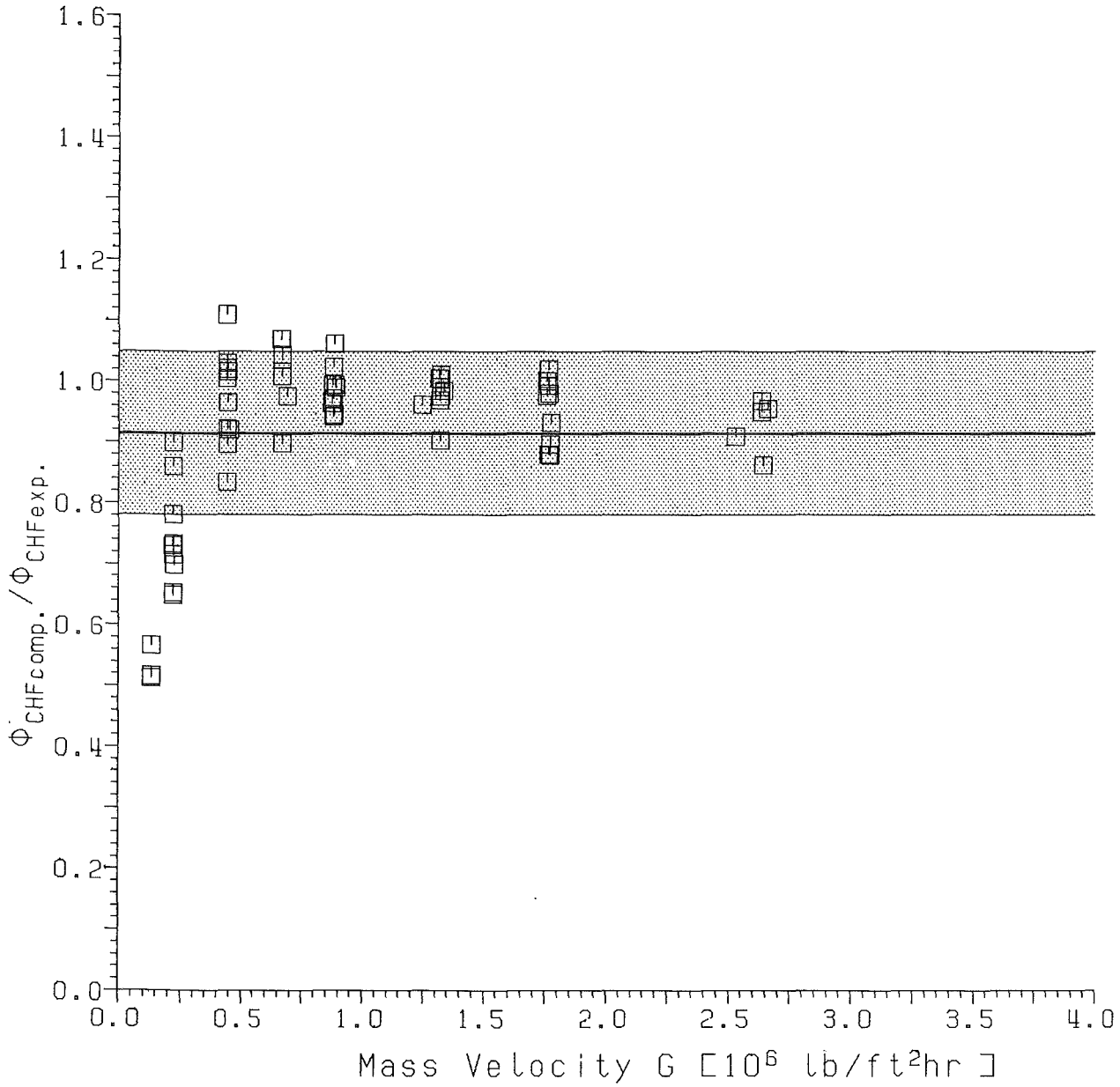

Fig.12 Spacer grid data (Table 14, F_G=0.88775) φ vs. G for standard Q-values and optimum V=V(G) function.

Experimental Data

Table	:	14
Number of data points	:	60

optimum function $v(g) = 3.1-(1.15-.1188*g)*g+2.5*\exp(-g)$

Geometry dependent constants

Q1	:	1.763
Q2	:	9.157
Q4	:	6.507

Results

Mean error	:	-8.57	%
Standard deviation	:	13.41	%
RMS-error	:	15.91	%
lower limit	:	-48.67	%
upper limit	:	10.91	%

Comments to Fig. 12.

Tables : 1, 2, 3, 4, 5, 6, 7, 8, 9, 10, 11, 12, 13

Q_1 = 1.763 $\quad\quad$ $\bar{e}$ = 2.38 %

Q_2 = 9.157 $\quad\quad$ σ = 11.41 %

Q_4 = 6.507 $\quad\quad$ ε_{RMS} = 11.65 %

$V = 3.1-1.15*G+0.1188*G^2-2.5*\exp(-G)$

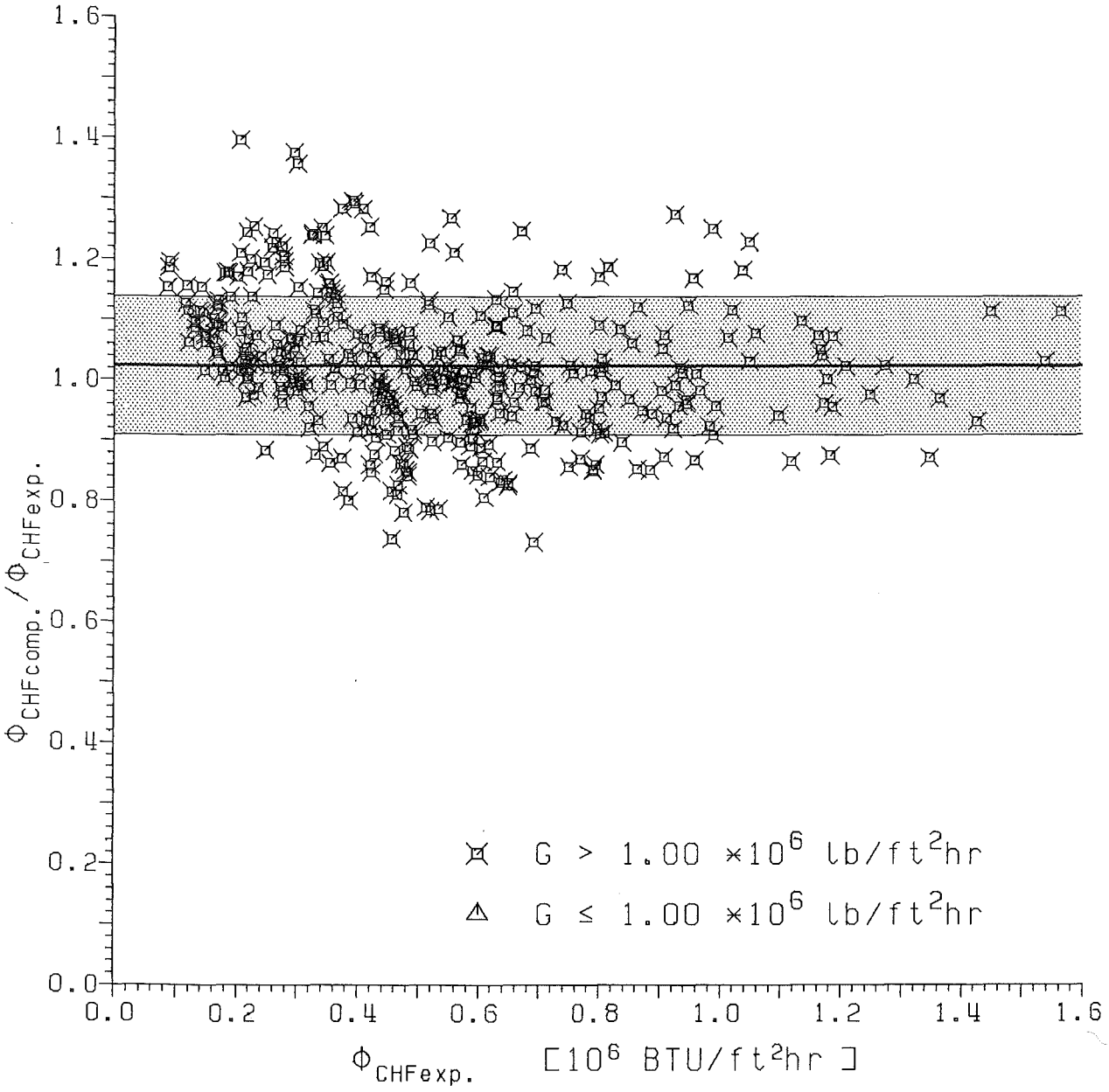

Fig.13 Spacer grid data (Table 1-13) φ vs. G for G>10^6 lb/ft^{2}hr.

Tables : 1, 2, 3, 4, 5, 6, 7, 8, 9, 10 11, 12, 13

$Q_1 = 1.763$ $\quad \bar{e} = 4.53$ %

$Q_2 = 9.157$ $\quad \sigma = 11.04$ %

$Q_4 = 6.507$ $\quad \varepsilon_{RMS} = 11.93$ %

$V = 3.1-1.15*G+0.1188*G^2-2.5*\exp(-G)$

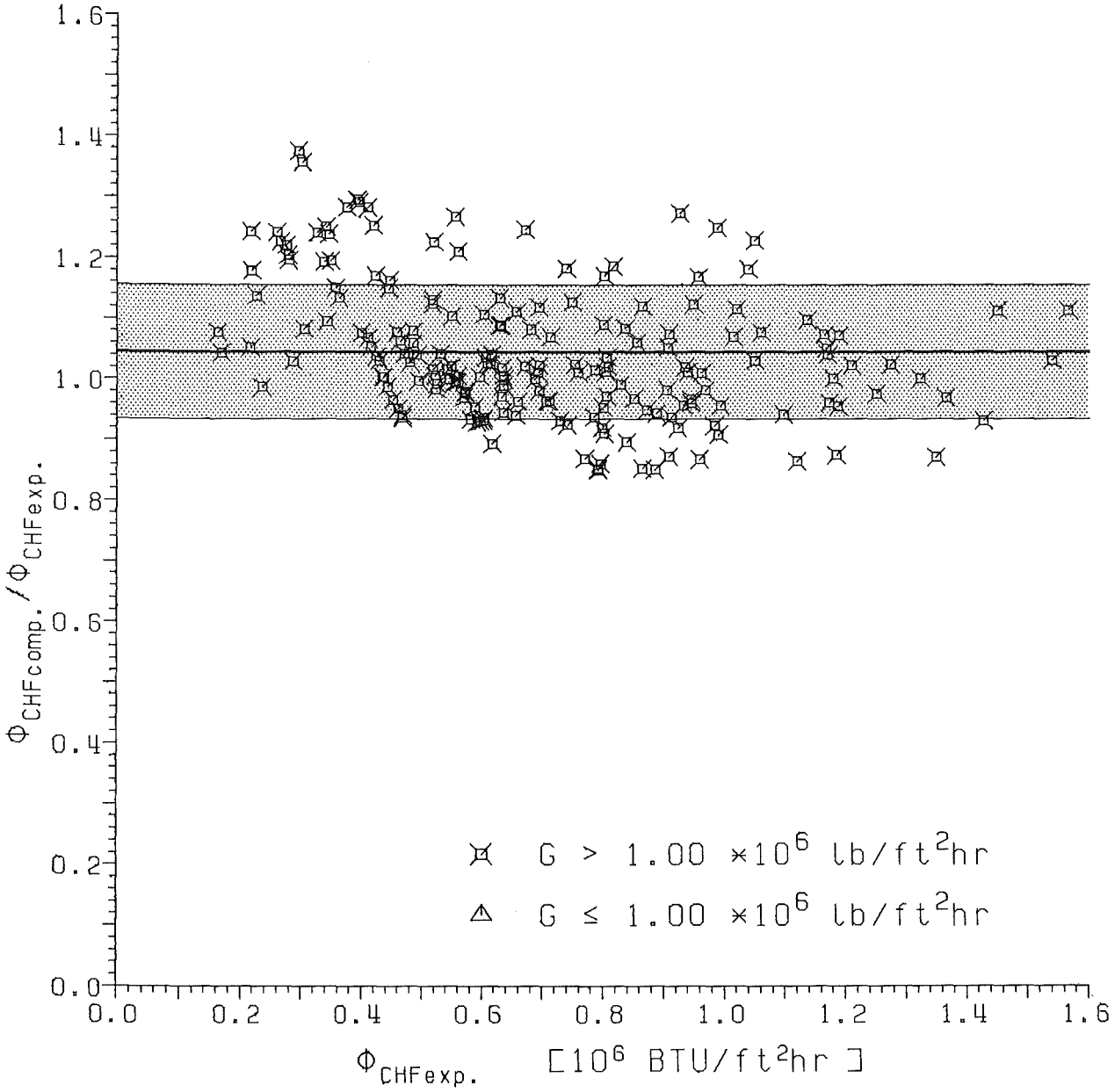

Fig.14 Spacer grid data (Table 1-13) φ vs. G for $G>10^6$ lb/ft²hr and $x<0.05$.

Tables : 1, 2, 3, 4, 5, 6, 7, 8, 9, 10 11, 12, 13

Q_1 = 1.763 $\quad\quad$ $\bar{e}$ = 2.38 %

Q_2 = 9.157 $\quad\quad$ σ = 11.41 %

Q_4 = 6.507 $\quad\quad$ ε_{RMS} = 11.65 %

$V = 3.1-1.15*G+0.1188*G^2-2.5*\exp(-G)$

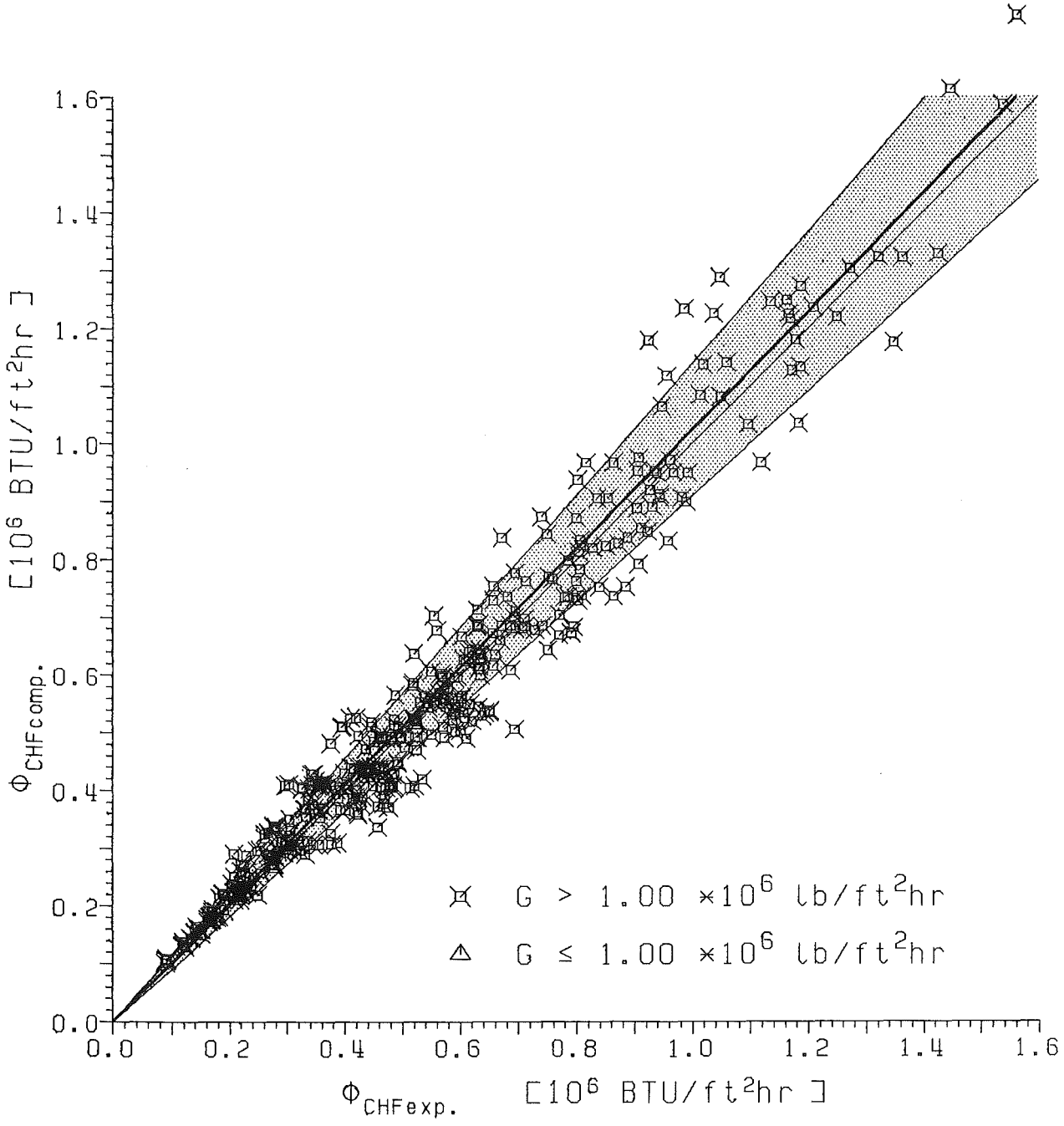

Fig.15 Spacer grid data (Table 1-13) $\Phi_{CHFcomp.}$ vs. $\Phi_{CHFexp.}$ for $G>10^6$ lb/ft²hr.

Tables : 1, 2, 3, 4, 5, 6, 7, 8, 9, 10 11, 12, 13

Q_1 = 1.763 $\quad\quad$ $\bar{e}$ = 4.53 %

Q_2 = 9.157 $\quad\quad$ σ = 11.04 %

Q_4 = 6.507 $\quad\quad$ ε_{RMS} = 11.93 %

$V = 3.1-1.15*G+0.1188*G^2+2.5*\exp(-G)$

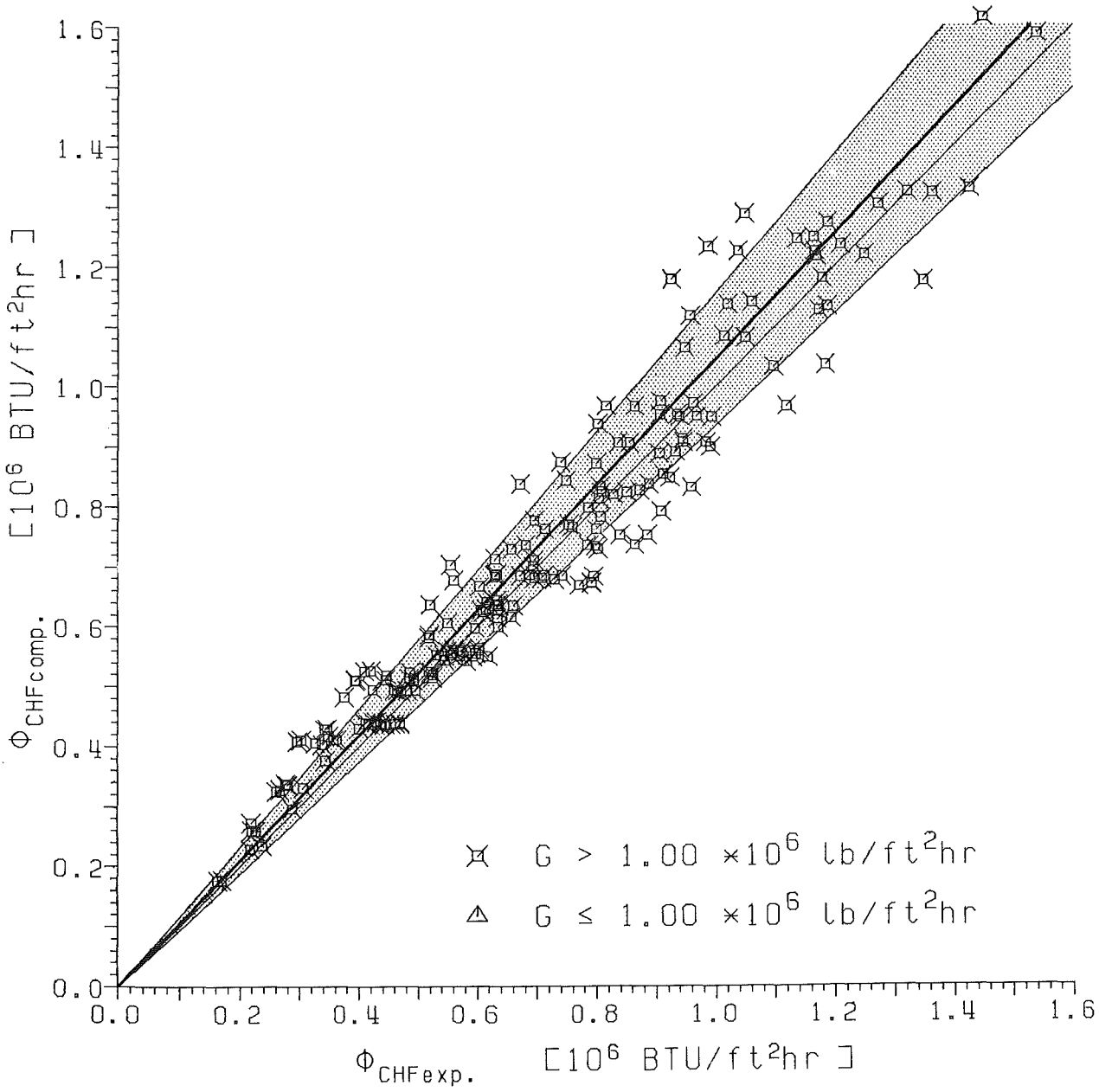

Fig.16 Spacer grid data (Table 1-13) $\Phi_{CHFcomp.}$ vs. $\Phi_{CHFexp.}$ for $G>10^6$ lb/ft²hr and $x<0.05$.

$Q_1 = 1.763$ $\quad Z = 53.75$ in

$F_p = 1.000$

$Q_2 = 9.157$ $\quad d_h = 0.2599$ in

$Y = 1.$

$Q_4 = 6.507$ $\quad p = 1200$ p.s.i.a.

$$V = 3.1-1.15*G+0.1188*G^2-2.5*\exp(-G)$$

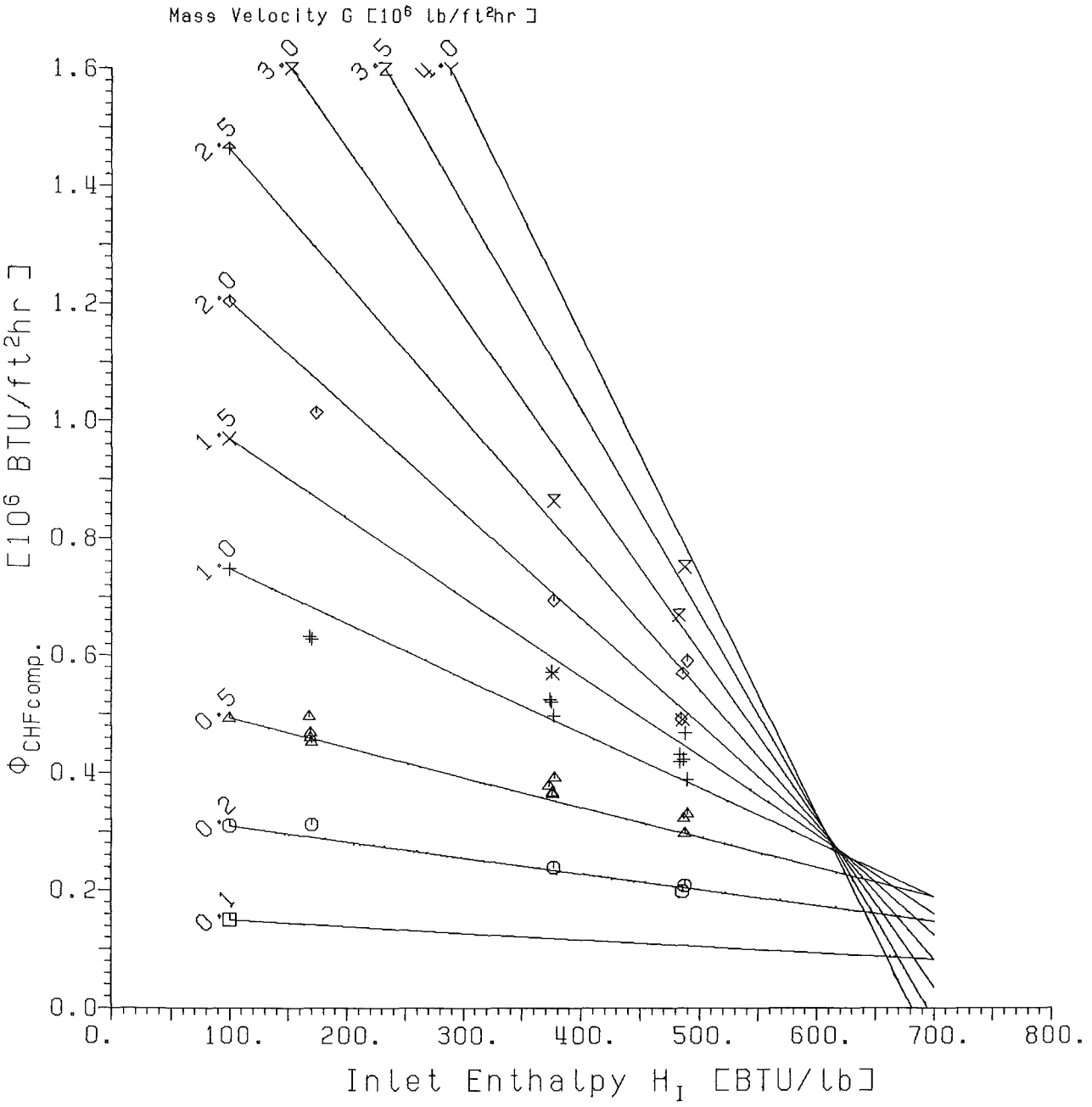

Fig.17 Critical heat flux vs. inlet enthalpy and mass velocity spacer grid, p=1200 p.s.i.a., uniform heat flux distribution (Tables 5,8,9).

$Q_1 = 1.763$

$Q_2 = 9.157$

$Q_4 = 6.507$

$Z = 53.75$ in

$F_p = 1.000$

$d_h = 0.2599$ in

$Y = 1.$

$p = 1600$ p.s.i.a.

$$V = 3.1 - 1.15 \times G + 0.1188 \times G^2 + 2.5 \times \exp(-G)$$

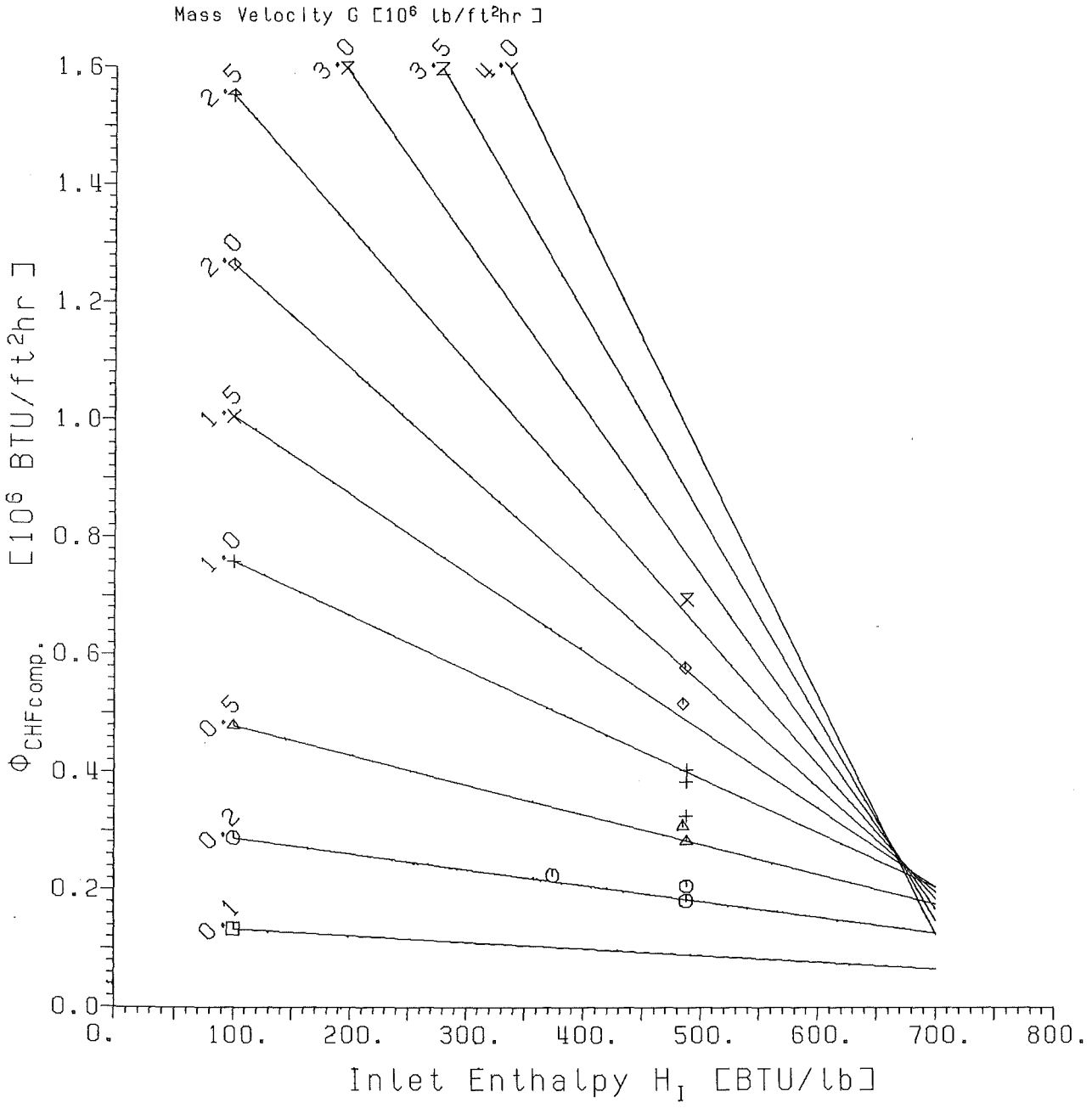

Fig.18 Critical heat flux vs. inlet enthalpy and mass velocity spacer grid, p=1600 p.s.i.a., uniform heat flux distribution (Tables 5,8,9).

$Q_1 = 1.763$

$Q_2 = 9.157$

$Q_4 = 6.507$

$Z = 53.75$ in

$F_p = 1.000$

$d_h = 0.2599$ in

$Y = 1.$

$p = 2000$ p.s.i.a.

$$V = 3.1 - 1.15 \times G + 0.1188 \times G^2 + 2.5 \times \exp(-G)$$

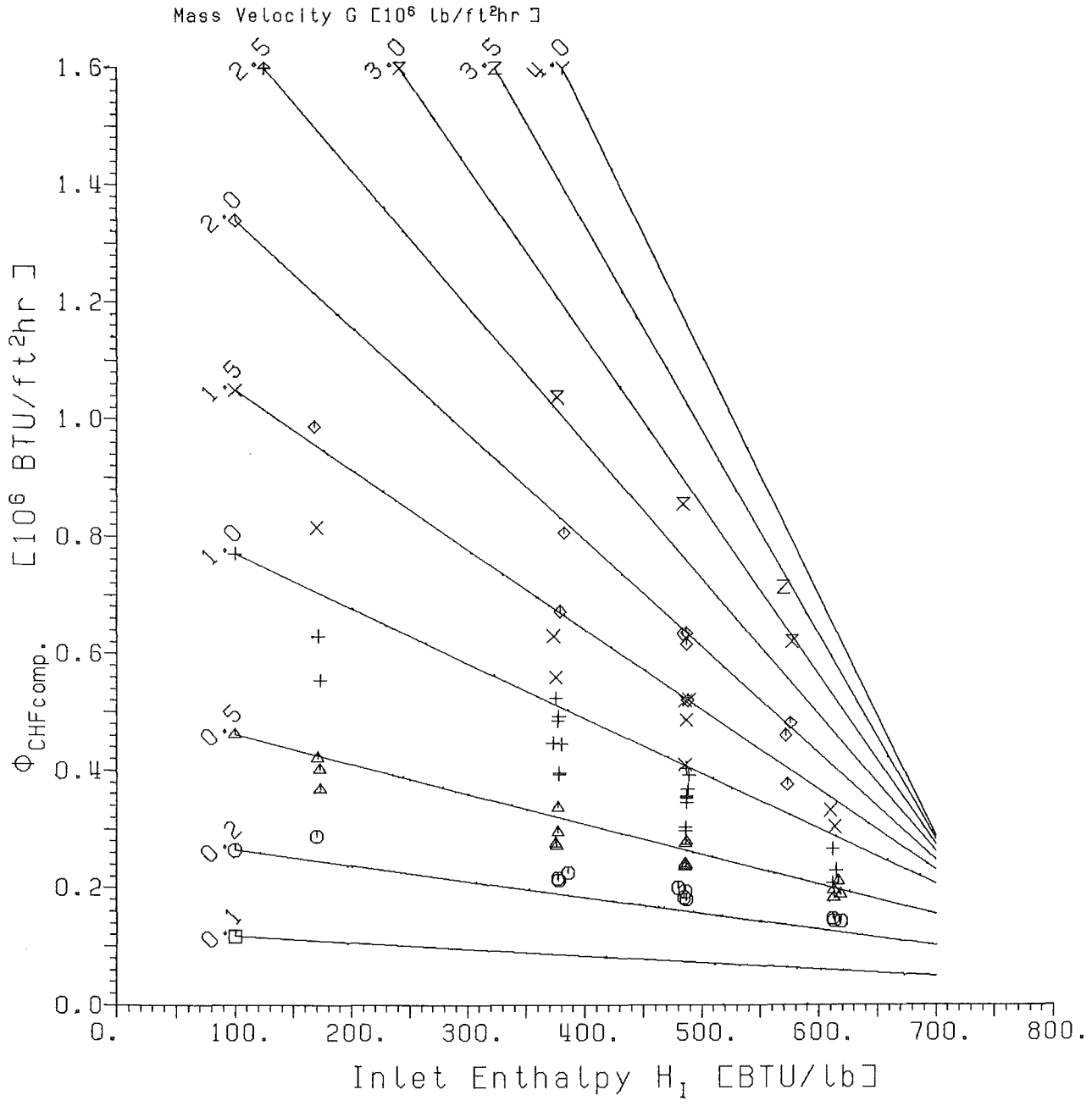

Fig.19 Critical heat flux vs. inlet enthalpy and mass velocity spacer grid, p=2000 p.s.i.a., uniform heat flux distribution (Tables 5,8,9).

Q_1 = 1.763

Q_2 = 9.157

Q_4 = 6.507

Z	=	53.75	in
F_p	=	1.091	
d_h	=	0.2599	in
Y	=	1.	
p	=	1200	p.s.i.a.

$V = 3.1-1.15*G+0.1188*G^2-2.5*\exp(-G)$

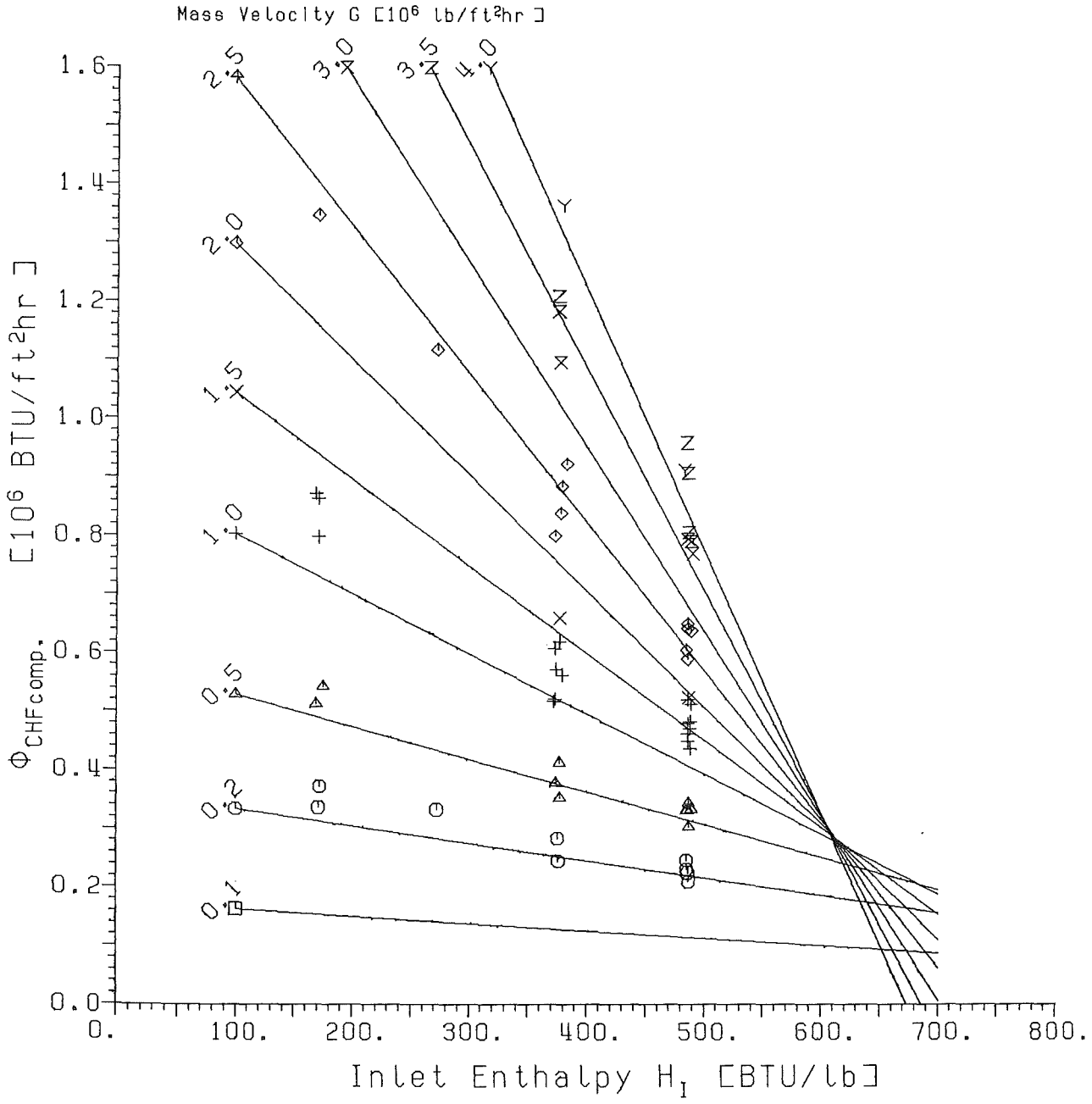

Fig.20 Critical heat flux vs. inlet enthalpy and mass velocity spacer grid, p=1200 p.s.i.a., non uniform heat flux distribution (Tables 3,4,6,7).

$Q_1 = 1.763$ $\quad$ $z = 53.75$ in

$F_p = 1.091$

$Q_2 = 9.157$ $\quad$ $d_h = 0.2599$ in

$\gamma = 1.$

$Q_4 = 6.507$ $\quad$ $p = 1600$ p.s.i.a.

$$V = 3.1-1.15\times G+0.1188\times G^2-2.5\times \exp(-G)$$

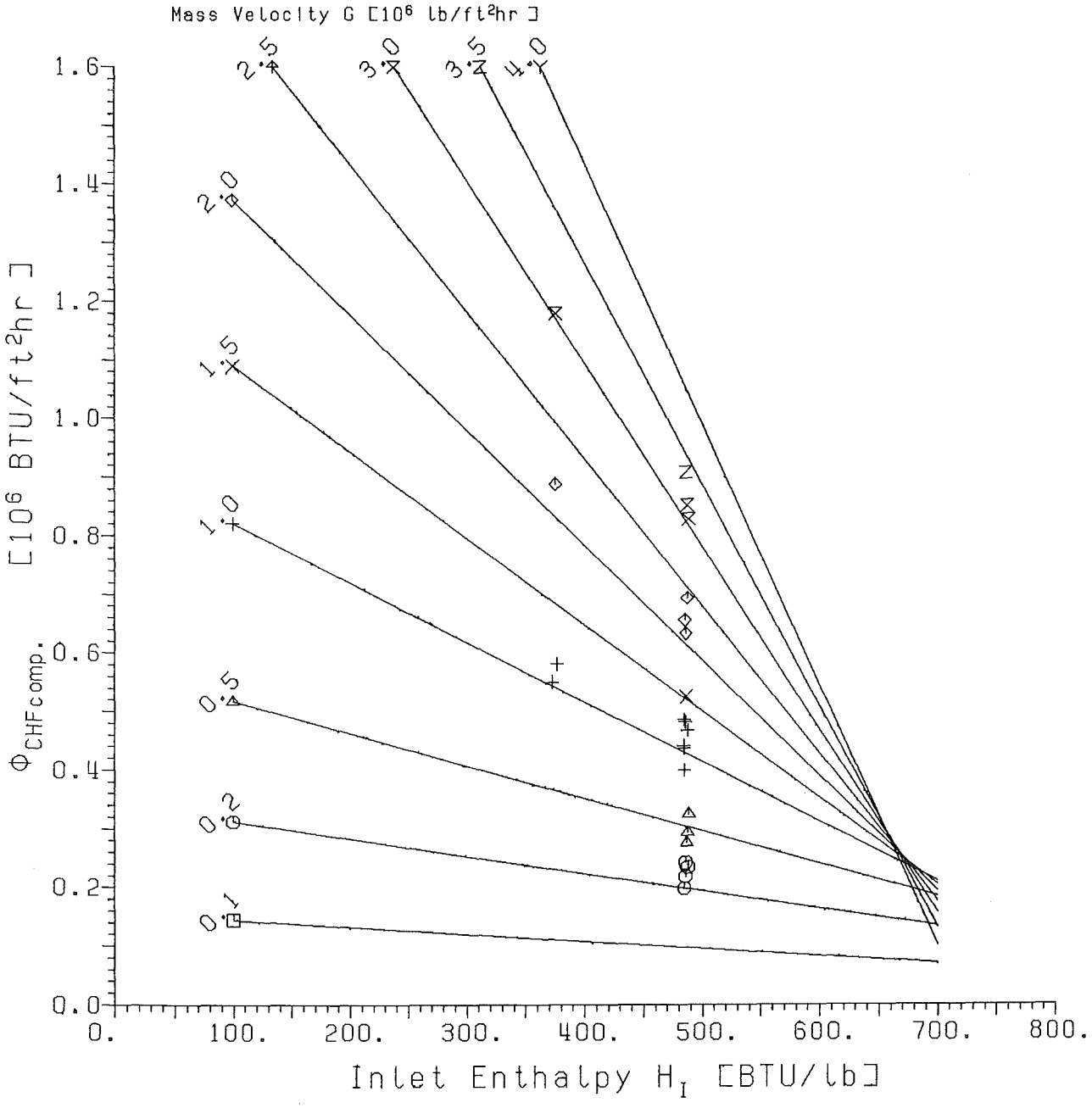

Fig.21 Critical heat flux vs. inlet enthalpy and mass velocity spacer grid, p=1600 p.s.i.a., non uniform heat flux distribution (Tables 3,4,6,7).

$Q_1 = 1.763$ $\quad$ $Z = 53.75$ in

$F_p = 1.091$

$Q_2 = 9.157$ $\quad$ $d_h = 0.2599$ in

$Y = 1.$

$Q_4 = 6.507$ $\quad$ $p = 2000$ p.s.i.a.

$V = 3.1-1.15*G+0.1188*G^2-2.5*\exp(-G)$

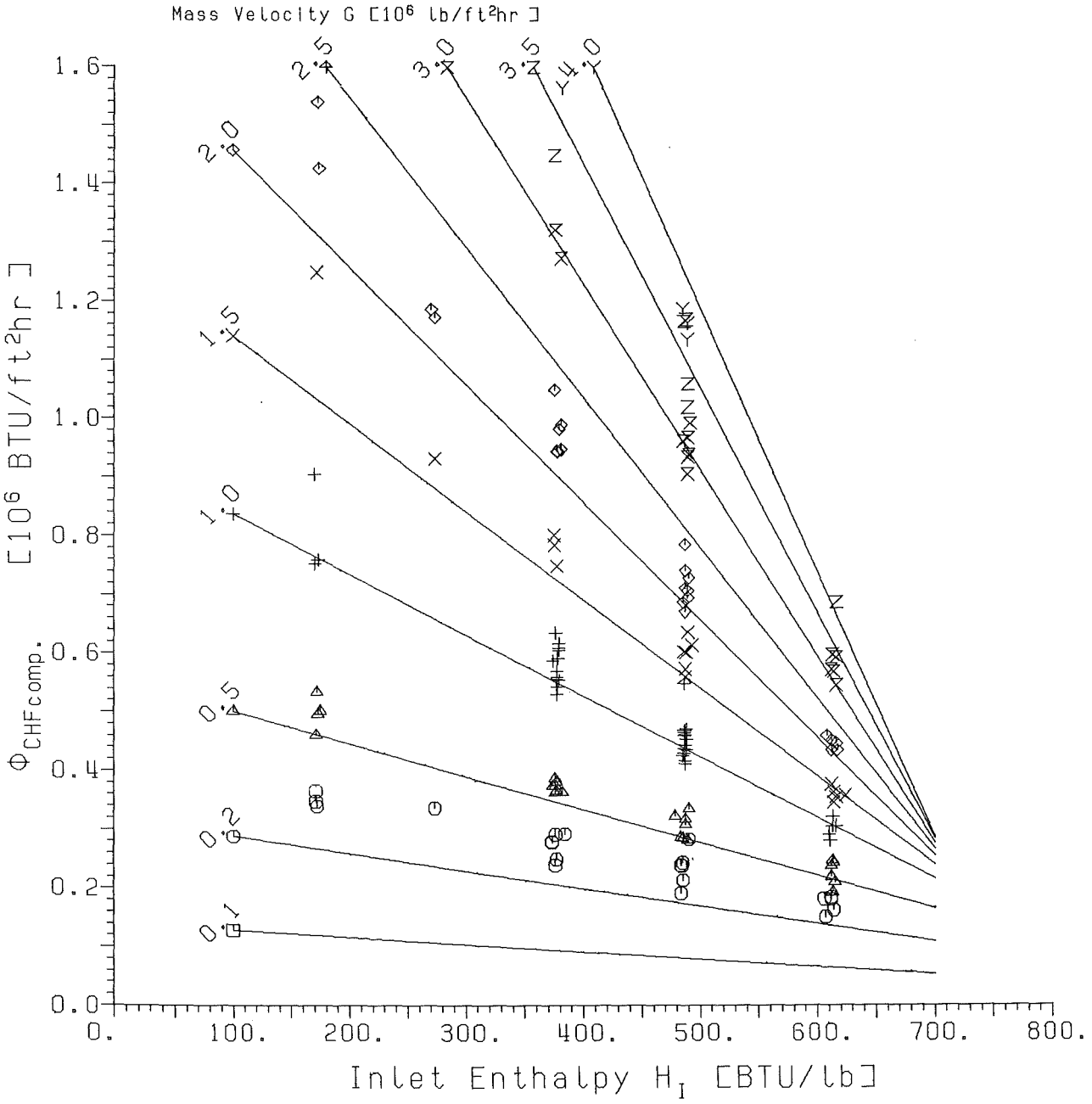

Fig.22 Critical heat flux vs. inlet enthalpy and mass velocity spacer grid, p=2000 p.s.i.a., non uniform heat flux distribution (Tables 3,4,6,7).

Q_1 = 1.763 | Z = 17.00 in | F_p = 1.000

Q_2 = 9.157 | d_h = 0.0903 in | Y = 1.

Q_4 = 6.507 | p = 1200 p.s.i.a.

$$V = 1-(025+0.1*G+2.75*\exp(-4*G)-3*\exp(-3*G))$$

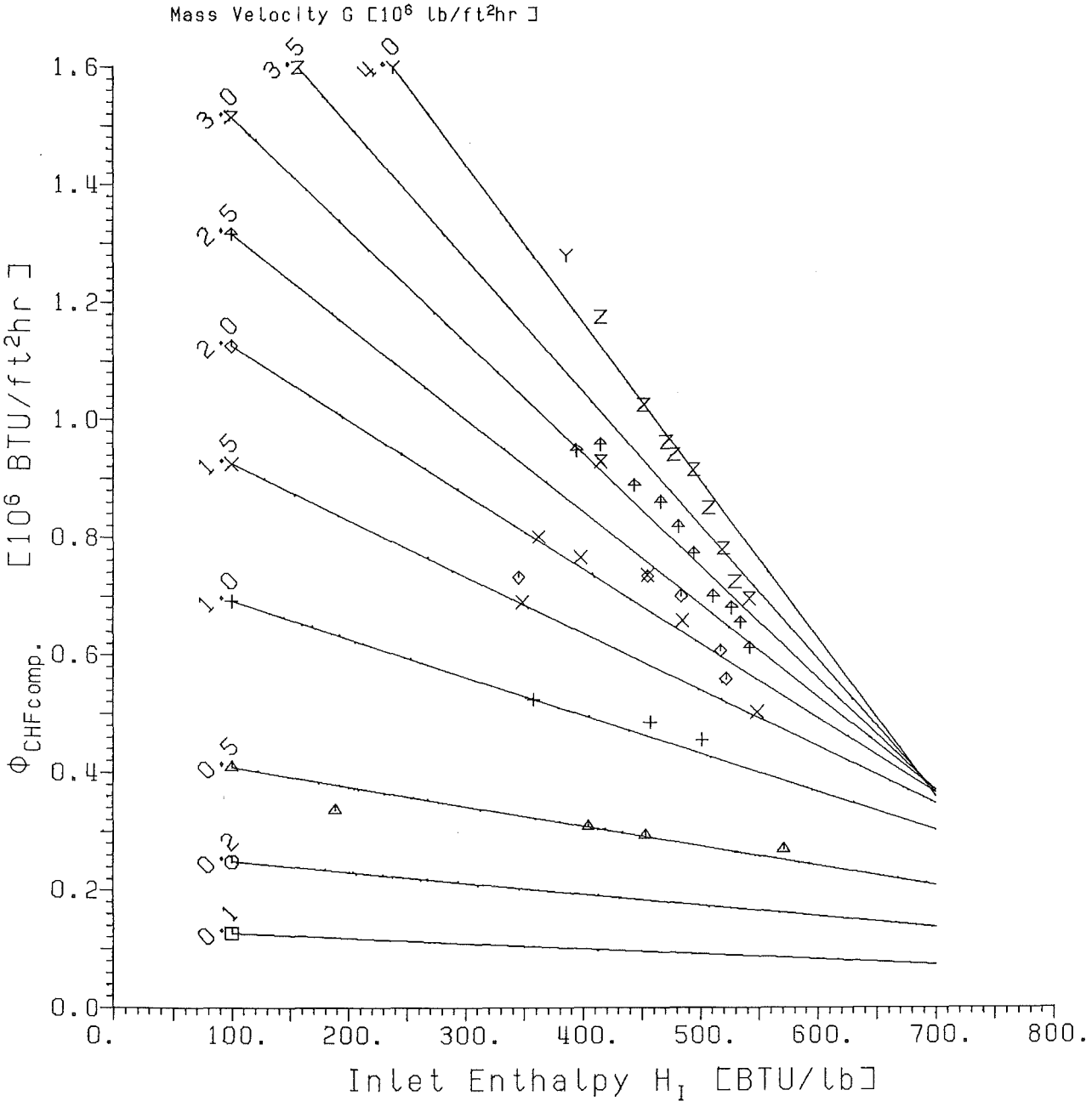

Fig.23 Critical heat flux vs. inlet enthalpy and mass velocity spiral rib spacer, p=1200 p.s.i.a., uniform heat flux distribution (Table 15).

TABLE NO.: 1
****

Z =	93.75
FP =	1.091
DH =	0.1104
Y =	1.
FG =	1.0686

TABLE : 1- 1

PRESSURE P PSIA	INLET ENTHALPY HIN BTU/LB	MASS VELOCITY G LB/H/SQFT *1.E-6	MAXIMUM HEAT FLUX PHI BTU/H/SQFT *1.E-6	AV. EXIT ENTHALPY HEX BTU/LB	AV. STEAM QUALITY
2000.	616.	0.255	0.047	970.	0.642
2000.	490.	0.256	0.058	929.	0.554
2000.	375.	0.257	0.067	883.	0.455
2000.	171.	0.258	0.091	851.	0.386
2000.	609.	0.513	0.068	865.	0.416
2000.	489.	0.512	0.085	811.	0.300
2000.	377.	0.512	0.103	768.	0.207
2000.	171.	0.516	0.138	688.	0.035
2000.	613.	1.024	0.091	786.	0.246
2000.	617.	1.001	0.090	791.	0.257
2000.	489.	1.022	0.133	740.	0.147
2000.	486.	1.024	0.132	735.	0.136
2000.	371.	1.028	0.170	682.	0.022
2000.	376.	1.028	0.164	684.	0.026
2000.	173.	1.031	0.237	618.	-0.116
2000.	614.	1.503	0.119	767.	0.205
2000.	485.	1.509	0.170	703.	0.067
2000.	381.	1.478	0.218	666.	-0.013
2000.	613.	1.986	0.143	753.	0.175
2000.	484.	2.010	0.222	697.	0.054
2000.	374.	2.010	0.288	651.	-0.045
2000.	596.	3.050	0.204	725.	0.114
2000.	486.	3.010	0.306	683.	0.024
1600.	486.	0.255	0.058	928.	0.564
1600.	376.	0.257	0.068	891.	0.496
1600.	490.	0.512	0.086	817.	0.358
1600.	375.	0.514	0.104	768.	0.267
1600.	486.	1.028	0.140	749.	0.232
1600.	377.	1.026	0.170	698.	0.137
1600.	486.	1.503	0.171	707.	0.154
1600.	488.	2.010	0.210	691.	0.124
1600.	486.	3.000	0.292	674.	0.093
1200.	488.	0.256	0.056	910.	0.553
1200.	374.	0.257	0.067	876.	0.497
1200.	168.	0.258	0.088	824.	0.412
1200.	484.	0.512	0.091	828.	0.419
1200.	374.	0.514	0.103	761.	0.309
1200.	170.	0.508	0.128	660.	0.144
1200.	490.	1.027	0.145	763.	0.313
1200.	375.	1.027	0.172	699.	0.208
1200.	169.	1.031	0.234	608.	0.059
1200.	485.	1.503	0.190	729.	0.257
1200.	377.	1.504	0.231	673.	0.166
1200.	485.	2.010	0.219	696.	0.203
1200.	485.	2.010	0.219	696.	0.203
1200.	375.	2.010	0.280	644.	0.118
1200.	484.	3.010	0.275	661.	0.146
1200.	385.	2.990	0.363	620.	0.079

TABLE NO.: 2
****

Z =	93.75
FP =	1.000
DH =	0.1104
Y =	1.
FG =	1.0686

TABLE : 2- 1

PRESSURE P PSIA	INLET ENTHALPY HIN BTU/LB	MASS VELOCITY G LB/H/SQFT *1.E-6	MAXIMUM HEAT FLUX PHI BTU/H/SQFT *1.E-6	AV. EXIT ENTHALPY HEX BTU/LB	AV. STEAM QUALITY
**********	**********	**********	**********	**********	**********
2000.	613.	0.259	0.040	1056.	0.827
2000.	490.	0.254	0.050	1063.	0.842
2000.	378.	0.257	0.061	1065.	0.847
2000.	377.	0.257	0.059	1043.	0.799
2000.	174.	0.259	0.077	1038.	0.789
2000.	585.	0.522	0.063	932.	0.560
2000.	482.	0.512	0.079	930.	0.556
2000.	380.	0.514	0.095	916.	0.526
2000.	378.	0.512	0.095	913.	0.519
2000.	173.	0.515	0.125	876.	0.440
2000.	612.	1.022	0.088	863.	0.412
2000.	485.	1.025	0.121	827.	0.334
2000.	486.	1.006	0.118	825.	0.330
2000.	381.	1.022	0.150	806.	0.289
2000.	379.	1.008	0.150	812.	0.302
2000.	186.	1.027	0.209	776.	0.224
2000.	613.	1.508	0.122	848.	0.379
2000.	487.	1.509	0.168	811.	0.300
2000.	375.	1.527	0.219	791.	0.257
2000.	172.	1.518	0.295	736.	0.138
2000.	607.	2.020	0.149	821.	0.321
2000.	482.	2.020	0.221	799.	0.274
2000.	377.	2.010	0.278	778.	0.229
2000.	614.	2.690	0.177	805.	0.287
2000.	483.	3.020	0.297	768.	0.207
1600.	488.	0.258	0.052	1074.	0.835
1600.	379.	0.256	0.061	1072.	0.831
1600.	485.	0.511	0.087	978.	0.657
1600.	376.	0.514	0.103	959.	0.622
1600.	176.	0.514	0.136	941.	0.588
1600.	485.	1.025	0.133	861.	0.440
1600.	374.	1.025	0.162	833.	0.388
1600.	486.	1.512	0.167	806.	0.338
1600.	376.	1.512	0.215	788.	0.304
1600.	485.	1.973	0.213	798.	0.323
1600.	377.	2.010	0.275	774.	0.278
1600.	488.	2.820	0.273	768.	0.267
1200.	486.	0.258	0.053	1087.	0.842
1200.	376.	0.256	0.063	1093.	0.852
1200.	171.	0.259	0.079	1050.	0.781
1200.	489.	0.512	0.097	1039.	0.763
1200.	373.	0.512	0.114	1016.	0.726
1200.	170.	0.515	0.139	954.	0.625
1200.	491.	1.022	0.149	914.	0.559
1200.	377.	1.027	0.178	881.	0.505
1200.	173.	1.028	0.225	808.	0.386
1200.	490.	1.512	0.182	839.	0.437
1200.	373.	1.500	0.230	817.	0.401
1200.	171.	1.512	0.298	742.	0.278
1200.	489.	2.150	0.249	825.	0.414
1200.	377.	2.010	0.277	777.	0.335

TABLE NO.: 3
****

Z =	53.75
FP =	1.091
DH =	0.2599
Y =	1.
FG =	1.0068

TABLE : 3- 1

PRESSURE P PSIA	INLET ENTHALPY HIN BTU/LB	MASS VELOCITY G LB/H/SQFT *1.E-6	MAXIMUM HEAT FLUX PHI BTU/H/SQFT *1.E-6	AV. EXIT ENTHALPY HEX BTU/LB	AV. STEAM QUALITY
**********	**********	**********	**********	**********	**********
2000.	612.	0.249	0.183	909.	0.511
2000.	484.	0.250	0.238	870.	0.427
2000.	376.	0.250	0.291	848.	0.379
2000.	273.	0.251	0.336	816.	0.310
2000.	614.	0.498	0.242	812.	0.302
2000.	487.	0.499	0.317	745.	0.158
2000.	490.	0.498	0.335	762.	0.194
2000.	377.	0.500	0.381	686.	0.030
2000.	616.	1.001	0.305	739.	0.145
2000.	617.	0.992	0.342	757.	0.183
2000.	487.	0.997	0.416	656.	-0.034
2000.	486.	1.008	0.429	659.	-0.028
2000.	487.	0.999	0.461	674.	0.005
2000.	487.	0.998	0.468	678.	0.013
2000.	377.	0.998	0.570	609.	-0.135
2000.	616.	1.492	0.354	712.	0.086
2000.	486.	1.487	0.549	636.	-0.077
2000.	616.	1.995	0.446	706.	0.074
2000.	485.	1.990	0.687	625.	-0.101
2000.	616.	2.990	0.593	696.	0.052
2000.	490.	3.000	0.939	617.	-0.118
2000.	616.	3.500	0.687	696.	0.052
2000.	485.	4.030	1.188	605.	-0.144
1600.	488.	0.250	0.234	867.	0.451
1600.	489.	0.498	0.324	753.	0.239
1600.	485.	0.999	0.486	683.	0.110
1200.	485.	0.250	0.231	861.	0.473
1200.	375.	0.250	0.283	835.	0.430
1200.	273.	0.248	0.341	830.	0.422
1200.	489.	0.499	0.333	760.	0.308
1200.	377.	0.503	0.413	710.	0.226
1200.	270.	0.496	0.465	650.	0.128
1200.	486.	0.997	0.480	682.	0.180
1200.	488.	0.998	0.483	684.	0.184
1200.	377.	0.999	0.620	629.	0.094
1200.	277.	0.991	0.735	578.	0.010
1200.	489.	1.997	0.638	618.	0.076
1200.	490.	2.990	0.770	594.	0.037
1200.	485.	3.910	0.959	585.	0.022
2000.	606.	0.251	0.181	898.	0.487
2000.	483.	0.249	0.239	872.	0.431
2000.	373.	0.252	0.278	820.	0.319
2000.	273.	0.247	0.324	805.	0.287
2000.	171.	0.254	0.365	753.	0.175
2000.	612.	0.498	0.237	805.	0.287
2000.	478.	0.500	0.323	740.	0.147
2000.	377.	0.498	0.366	675.	0.007
2000.	273.	0.495	0.438	632.	-0.086
2000.	171.	0.502	0.461	543.	-0.277
2000.	613.	0.994	0.305	737.	0.140
2000.	486.	0.995	0.437	664.	-0.017
2000.	487.	0.995	0.443	668.	-0.008
2000.	485.	0.954	0.447	675.	0.007
2000.	377.	0.999	0.531	592.	-0.172
2000.	378.	0.999	0.543	599.	-0.157

TABLE : 3- 2

PRESSURE P PSIA	INLET ENTHALPY HIN BTU/LB	MASS VELOCITY G LB/H/SQFT *1.E-6	MAXIMUM HEAT FLUX PHI BTU/H/SQFT *1.E-6	AV. EXIT ENTHALPY HEX BTU/LB	AV. STEAM QUALITY
**********	**********	**********	**********	**********	**********
2000.	272.	0.989	0.633	532.	-0.301
2000.	273.	0.993	0.635	532.	-0.301
2000.	170.	1.003	0.753	475.	-0.424
2000.	487.	1.495	0.573	643.	-0.062
2000.	487.	2.000	0.671	623.	-0.105
2000.	489.	3.000	0.906	603.	-0.148
2000.	489.	4.000	1.136	604.	-0.146
1600.	486.	0.250	0.242	878.	0.471
1600.	486.	0.486	0.327	759.	0.251
1600.	486.	0.996	0.482	682.	0.108
1200.	485.	0.249	0.246	886.	0.514
1200.	272.	0.249	0.332	812.	0.393
1200.	487.	0.499	0.344	766.	0.318
1200.	267.	0.496	0.510	684.	0.184
1200.	486.	0.998	0.521	698.	0.206
1200.	280.	0.990	0.740	583.	0.019

TABLE NO.: 4
****

Z =	53.75
FP =	1.091
DH =	0.2599
Y =	1.
FG =	1.0068

TABLE : 4- 1

PRESSURE P PSIA	INLET ENTHALPY HIN BTU/LB	MASS VELOCITY G LB/H/SQFT *1.E-6	MAXIMUM HEAT FLUX PHI BTU/H/SQFT *1.E-6	AV. EXIT ENTHALPY HEX BTU/LB	AV. STEAM QUALITY
**********	**********	**********	**********	**********	**********
2000.	612.	0.250	0.180	904.	0.500
2000.	490.	0.249	0.283	869.	0.425
2000.	384.	0.250	0.292	857.	0.399
2000.	613.	0.500	0.246	813.	0.304
2000.	489.	0.499	0.282	718.	0.099
2000.	376.	0.501	0.363	670.	-0.004
2000.	613.	0.997	0.321	744.	0.155
2000.	486.	1.001	0.468	676.	0.009
2000.	374.	1.013	0.588	610.	-0.133
2000.	379.	1.000	0.617	629.	-0.092
2000.	614.	1.496	0.345	703.	0.067
2000.	486.	1.503	0.603	649.	-0.049
2000.	375.	1.512	0.785	586.	-0.185
2000.	273.	1.512	0.932	523.	-0.321
2000.	612.	2.000	0.435	700.	0.061
2000.	487.	2.000	0.711	632.	-0.086
2000.	490.	2.000	0.729	638.	-0.073
2000.	379.	2.010	0.983	578.	-0.202
2000.	273.	2.020	1.173	509.	-0.351
2000.	174.	2.020	1.427	461.	-0.454
2000.	612.	3.000	0.572	689.	0.037
2000.	489.	3.000	0.935	615.	-0.122
2000.	491.	3.010	0.993	625.	-0.101
2000.	376.	3.020	1.323	554.	-0.254
2000.	486.	3.880	1.167	608.	-0.137
2000.	382.	4.020	1.565	540.	-0.284
1600.	488.	1.001	0.467	677.	0.098
1600.	377.	1.005	0.581	611.	-0.024
1600.	486.	2.000	0.656	619.	-0.009
1600.	376.	2.010	0.888	555.	-0.128
1600.	489.	3.000	0.828	601.	-0.043
1600.	376.	3.010	1.179	534.	-0.167
1200.	489.	0.996	0.513	698.	0.206
1200.	373.	1.005	0.608	618.	0.076
1200.	171.	1.008	0.864	519.	-0.086
1200.	486.	1.994	0.642	617.	0.074
1200.	379.	2.010	0.885	557.	-0.024
1200.	272.	2.010	1.119	498.	-0.120
1200.	171.	2.020	1.349	442.	-0.212
1200.	489.	2.990	0.791	596.	0.040
1200.	376.	3.010	1.184	536.	-0.058
1200.	380.	4.010	1.365	518.	-0.088
2000.	612.	0.229	0.162	898.	0.487
2000.	487.	0.248	0.222	850.	0.384
2000.	373.	0.252	0.279	823.	0.326
2000.	171.	0.251	0.347	732.	0.130
2000.	612.	0.498	0.219	790.	0.254
2000.	483.	0.500	0.286	715.	0.093
2000.	374.	0.505	0.374	674.	0.005
2000.	173.	0.503	0.497	574.	-0.211
2000.	610.	0.976	0.299	734.	0.134
2000.	487.	1.001	0.411	654.	-0.038
2000.	485.	1.001	0.425	657.	-0.032
2000.	379.	1.005	0.555	603.	-0.148
2000.	377.	1.012	0.560	601.	-0.153

TABLE : 4- 2

PRESSURE P PSIA	INLET ENTHALPY HIN BTU/LB	MASS VELOCITY G LB/H/SQFT *1.E-6	MAXIMUM HEAT FLUX PHI BTU/H/SQFT *1.E-6	AV. EXIT ENTHALPY HEX BTU/LB	AV. STEAM QUALITY
**********	**********	**********	**********	**********	**********
2000.	173.	1.002	0.759	481.	-0.411
2000.	614.	1.494	0.363	713.	0.089
2000.	487.	1.503	0.560	638.	-0.073
2000.	617.	1.997	0.434	705.	0.071
2000.	489.	2.000	0.695	630.	-0.090
2000.	489.	2.000	0.707	632.	-0.086
2000.	378.	2.020	0.945	568.	-0.224
2000.	270.	2.020	1.187	509.	-0.351
2000.	616.	2.990	0.545	690.	0.039
2000.	485.	3.020	0.962	614.	-0.125
2000.	381.	3.010	1.274	553.	-0.256
2000.	489.	4.010	1.164	606.	-0.142
1200.	486.	0.250	0.225	852.	0.458
1200.	172.	0.252	0.372	773.	0.329
1200.	485.	0.497	0.332	756.	0.301
1200.	175.	0.501	0.543	615.	0.071
1200.	488.	0.995	0.471	680.	0.177
1200.	171.	1.002	0.798	494.	-0.127
1200.	486.	2.000	0.650	618.	0.076
1200.	378.	2.000	0.839	548.	-0.039
1200.	489.	3.000	0.791	596.	0.040
1200.	377.	3.010	1.097	525.	-0.076
1200.	483.	4.000	0.912	575.	0.006

TABLE NO.: 5
****

Z =	53.75
FP =	1.000
DH =	0.2599
Y =	1.
FG =	1.0068

TABLE : 5- 1

PRESSURE P PSIA	INLET ENTHALPY HIN BTU/LB	MASS VELOCITY G LB/H/SQFT *1.E-6	MAXIMUM HEAT FLUX PHI BTU/H/SQFT *1.E-6	AV. EXIT ENTHALPY HEX BTU/LB	AV. STEAM QUALITY
**********	**********	**********	**********	**********	**********
2000.	480.	0.250	0.200	966.	0.633
2000.	386.	0.249	0.226	938.	0.573
2000.	487.	0.499	0.279	827.	0.334
2000.	377.	0.508	0.337	781.	0.235
2000.	375.	1.002	0.524	693.	0.046
2000.	616.	0.248	0.153	991.	0.687
2000.	486.	0.251	0.194	955.	0.610
2000.	170.	0.251	0.288	868.	0.422
2000.	617.	0.497	0.211	875.	0.437
2000.	486.	0.501	0.275	820.	0.319
2000.	171.	0.503	0.422	682.	0.022
2000.	612.	0.997	0.266	774.	0.220
2000.	489.	0.998	0.392	728.	0.121
2000.	487.	1.009	0.404	731.	0.127
2000.	610.	1.501	0.332	745.	0.158
2000.	489.	1.499	0.521	700.	0.061
2000.	576.	2.090	0.481	716.	0.095
2000.	487.	2.000	0.635	681.	0.020
2000.	577.	3.070	0.620	700.	0.061
2000.	484.	3.010	0.855	657.	-0.032
2000.	570.	3.620	0.713	690.	0.039
1600.	488.	0.250	0.207	992.	0.683
1600.	485.	0.500	0.309	861.	0.440
1600.	488.	0.998	0.405	735.	0.206
1600.	487.	2.000	0.579	664.	0.074
1200.	486.	0.249	0.198	971.	0.652
1200.	377.	0.250	0.240	961.	0.636
1200.	170.	0.251	0.312	927.	0.580
1200.	490.	0.498	0.330	894.	0.527
1200.	378.	0.500	0.392	854.	0.461
1200.	168.	0.502	0.496	769.	0.322
1200.	488.	0.998	0.468	773.	0.329
1200.	375.	1.000	0.573	723.	0.247
1200.	490.	1.991	0.591	671.	0.162
1200.	488.	2.990	0.751	633.	0.100
2000.	619.	0.250	0.143	967.	0.636
2000.	487.	0.249	0.180	927.	0.549
2000.	378.	0.251	0.213	894.	0.478
2000.	619.	0.498	0.188	849.	0.382
2000.	486.	0.501	0.236	773.	0.218
2000.	376.	0.502	0.272	706.	0.074
2000.	618.	0.973	0.204	739.	0.145
2000.	612.	1.001	0.208	738.	0.142
2000.	487.	1.005	0.345	696.	0.052
2000.	487.	1.001	0.353	702.	0.065
2000.	487.	1.013	0.355	700.	0.061
2000.	373.	1.009	0.447	643.	-0.062
2000.	380.	1.005	0.445	656.	-0.034
2000.	377.	1.003	0.485	671.	-0.002
2000.	171.	1.012	0.630	550.	-0.262
2000.	487.	1.502	0.486	684.	0.026
2000.	373.	1.518	0.630	626.	-0.099
2000.	170.	1.517	0.816	498.	-0.374
2000.	572.	2.050	0.460	708.	0.078
2000.	487.	2.010	0.616	674.	0.005

TABLE : 5- 2

PRESSURE P PSIA	INLET ENTHALPY HIN BTU/LB	MASS VELOCITY G LB/H/SQFT *1.E-6	MAXIMUM HEAT FLUX PHI BTU/H/SQFT *1.E-6	AV. EXIT ENTHALPY HEX BTU/LB	AV. STEAM QUALITY
**********	**********	**********	**********	**********	**********
2000.	382.	2.010	0.806	626.	-0.099
2000.	168.	2.020	0.988	466.	-0.443
2000.	376.	3.020	1.038	585.	-0.187
1600.	488.	1.009	0.326	684.	0.111
1600.	485.	2.000	0.518	643.	0.035
1600.	488.	3.010	0.695	628.	0.007
1600.	488.	0.249	0.182	933.	0.573
1600.	374.	0.250	0.225	922.	0.553
1200.	488.	0.499	0.297	850.	0.455
1200.	376.	0.502	0.364	817.	0.401
1200.	169.	0.503	0.460	726.	0.252
1200.	490.	1.013	0.389	724.	0.249
1200.	484.	0.998	0.419	740.	0.275
1200.	377.	1.009	0.498	677.	0.172
1200.	168.	1.004	0.632	551.	-0.034
1200.	485.	2.000	0.492	635.	0.104
1200.	377.	2.010	0.695	587.	0.025
1200.	174.	2.020	1.014	480.	-0.150
1200.	483.	3.010	0.669	618.	0.076
1200.	377.	3.010	0.864	552.	-0.032

TABLE NO.: 6
****

Z =	53.75
FP =	1.091
DH =	0.2599
Y =	1.
FG =	1.0068

TABLE : 6- 1

PRESSURE P PSIA	INLET ENTHALPY HIN BTU/LB	MASS VELOCITY G LB/H/SQFT *1.E-6	MAXIMUM HEAT FLUX PHI BTU/H/SQFT *1.E-6	AV. EXIT ENTHALPY HEX BTU/LB	AV. STEAM QUALITY
**********	**********	**********	**********	**********	**********
2000.	614.	0.249	0.162	879.	0.446
2000.	485.	0.249	0.243	834.	0.349
2000.	375.	0.247	0.266	814.	0.306
2000.	171.	0.248	0.351	748.	0.164
2000.	615.	0.500	0.209	786.	0.246
2000.	485.	0.440	0.278	747.	0.162
2000.	377.	0.499	0.381	688.	0.035
2000.	175.	0.498	0.502	583.	-0.191
2000.	614.	0.965	0.312	746.	0.160
2000.	610.	1.000	0.291	729.	0.123
2000.	488.	0.995	0.435	667.	-0.010
2000.	488.	1.000	0.453	673.	0.002
2000.	380.	0.990	0.576	617.	-0.118
2000.	378.	0.995	0.592	620.	-0.112
2000.	377.	1.000	0.556	604.	-0.146
2000.	184.	0.990	0.842	530.	-0.305
2000.	624.	1.490	0.357	722.	0.108
2000.	488.	1.502	0.602	652.	-0.043
2000.	375.	1.495	0.802	594.	-0.168
2000.	608.	2.000	0.459	702.	0.065
2000.	487.	2.000	0.741	638.	-0.073
2000.	381.	2.000	0.990	583.	-0.191
2000.	377.	2.000	0.945	569.	-0.221
2000.	613.	3.000	0.597	694.	0.048
2000.	489.	2.990	0.968	622.	-0.107
2000.	488.	3.880	1.170	611.	-0.131
1600.	486.	0.249	0.218	842.	0.405
1600.	488.	0.498	0.293	728.	0.193
1600.	485.	1.000	0.441	665.	0.076
1600.	485.	1.000	0.400	648.	0.045
1600.	487.	1.495	0.525	631.	0.013
1600.	487.	2.000	0.633	616.	-0.015
1600.	488.	3.000	0.851	604.	-0.037
1200.	489.	0.248	0.225	859.	0.469
1200.	372.	0.248	0.279	831.	0.424
1200.	170.	0.248	0.353	750.	0.291
1200.	486.	0.499	0.332	757.	0.303
1200.	374.	0.497	0.378	685.	0.185
1200.	169.	0.497	0.513	590.	0.030
1200.	486.	0.995	0.462	676.	0.170
1200.	486.	1.000	0.449	669.	0.159
1200.	374.	0.993	0.578	612.	0.066
1200.	373.	1.000	0.522	587.	0.025
1200.	372.	1.000	0.518	584.	0.020
1200.	487.	1.495	0.524	630.	0.095
1200.	377.	1.500	0.660	556.	-0.026
1200.	485.	1.990	0.605	609.	0.061
1200.	373.	2.000	0.800	537.	-0.057
1200.	486.	3.000	0.795	594.	0.037
1200.	486.	3.680	0.908	587.	0.025

TABLE NO.: 7
****

Z =	53.75
FP =	1.091
DH =	0.2599
Y =	1.
FG =	1.0650

TABLE : 7- 1

PRESSURE P PSIA	INLET ENTHALPY HIN BTU/LB	MASS VELOCITY G LB/H/SQFT *1.E-6	MAXIMUM HEAT FLUX PHI BTU/H/SQFT *1.E-6	AV. EXIT ENTHALPY HEX BTU/LB	AV. STEAM QUALITY
**********	**********	**********	**********	**********	**********
2010.	607.	0.288	0.150	851.	0.385
2005.	485.	0.286	0.213	834.	0.349
2002.	483.	0.286	0.191	794.	0.263
2000.	376.	0.286	0.239	767.	0.205
2000.	377.	0.285	0.249	786.	0.246
2010.	172.	0.288	0.339	723.	0.108
2005.	613.	0.574	0.192	770.	0.211
2000.	487.	0.572	0.308	739.	0.145
1990.	485.	0.574	0.284	717.	0.099
2002.	485.	0.572	0.285	718.	0.099
2005.	382.	0.572	0.363	679.	0.014
2000.	376.	0.571	0.387	695.	0.050
1998.	376.	0.571	0.374	683.	0.025
2005.	172.	0.575	0.534	607.	-0.141
2000.	611.	1.109	0.281	730.	0.125
1995.	488.	1.145	0.471	681.	0.021
2000.	486.	1.145	0.464	675.	0.007
2005.	486.	1.148	0.459	673.	0.001
2000.	379.	1.142	0.609	629.	-0.092
2000.	379.	1.151	0.606	626.	-0.099
1990.	376.	1.143	0.635	637.	-0.072
2000.	170.	1.152	0.905	537.	-0.290
2000.	612.	1.719	0.376	715.	0.093
2005.	493.	1.720	0.614	660.	-0.027
2000.	489.	1.717	0.636	663.	-0.019
2000.	377.	1.727	0.749	581.	-0.196
2000.	172.	1.725	1.250	512.	-0.344
1995.	612.	2.297	0.451	704.	0.070
2000.	487.	2.297	0.786	648.	-0.051
2000.	381.	2.301	0.948	574.	-0.211
2000.	375.	2.306	1.050	589.	-0.178
2000.	173.	2.303	1.540	488.	-0.396
2002.	614.	3.153	0.569	699.	0.058
1995.	489.	3.444	1.060	634.	-0.080
2000.	489.	3.425	1.020	628.	-0.094
2000.	375.	3.459	1.450	571.	-0.217
1602.	485.	0.291	0.198	805.	0.336
1595.	487.	0.572	0.276	713.	0.166
1605.	485.	1.145	0.437	664.	0.073
1605.	373.	1.142	0.550	599.	-0.048
1605.	488.	2.298	0.693	630.	0.010
1600.	487.	3.441	0.908	611.	-0.024
1200.	487.	0.285	0.210	832.	0.425
1205.	376.	0.284	0.245	781.	0.341
1200.	171.	0.286	0.336	720.	0.242
1200.	487.	0.571	0.303	736.	0.268
1195.	377.	0.569	0.353	667.	0.157
1198.	488.	1.142	0.437	667.	0.156
1200.	379.	1.153	0.563	608.	0.059
1205.	374.	1.141	0.573	610.	0.062
1200.	169.	1.151	0.872	524.	-0.078
1207.	486.	2.286	0.590	607.	0.056
1195.	383.	2.291	0.923	571.	0.000
1204.	487.	3.433	0.806	597.	0.041
1210.	376.	3.448	1.210	541.	-0.052

TABLE NO.: 8
****

Z =	53.75
FP =	1.000
DH =	0.2599
Y =	1.
FG =	1.0068

TABLE : 8- 1

PRESSURE P PSIA	INLET ENTHALPY HIN BTU/LB	MASS VELOCITY G LB/H/SQFT *1.E-6	MAXIMUM HEAT FLUX PHI BTU/H/SQFT *1.E-6	AV. EXIT ENTHALPY HEX BTU/LB	AV. STEAM QUALITY
**********	**********	**********	**********	**********	**********
2000.	612.	0.249	0.147	973.	0.649
2008.	485.	0.249	0.183	932.	0.560
2000.	380.	0.246	0.207	893.	0.476
2000.	172.	0.236	0.261	849.	0.382
2000.	613.	0.499	0.196	854.	0.392
2000.	486.	0.499	0.241	782.	0.237
2000.	377.	0.500	0.295	737.	0.140
2000.	173.	0.500	0.402	665.	-0.015
2000.	615.	0.966	0.245	771.	0.214
2000.	488.	0.995	0.368	715.	0.093
2000.	487.	0.998	0.357	706.	0.074
2000.	378.	1.000	0.492	679.	0.015
1995.	486.	1.497	0.519	698.	0.057
2000.	484.	2.003	0.633	677.	0.011
1595.	491.	0.232	0.192	997.	0.692
1595.	488.	0.498	0.283	836.	0.394
1603.	488.	0.996	0.385	724.	0.185
1200.	488.	0.251	0.208	994.	0.690
1205.	376.	0.248	0.233	952.	0.621
1195.	169.	0.246	0.299	911.	0.555
1195.	484.	0.495	0.323	883.	0.509
1200.	373.	0.499	0.378	836.	0.432
1200.	169.	0.500	0.468	742.	0.278
1195.	488.	0.992	0.437	758.	0.305
1205.	375.	0.998	0.522	695.	0.201

TABLE NO.: 9
****

Z =	53.75
FP =	1.000
DH =	0.2599
Y =	1.
FG =	1.0068

TABLE : 9- 1

PRESSURE P PSIA	INLET ENTHALPY HIN BTU/LB	MASS VELOCITY G LB/H/SQFT *1.E-6	MAXIMUM HEAT FLUX PHI BTU/H/SQFT *1.E-6	AV. EXIT ENTHALPY HEX BTU/LB	AV. STEAM QUALITY
**********	**********	**********	**********	**********	**********
2000.	613.	0.249	0.143	964.	0.629
2000.	487.	0.248	0.181	933.	0.562
2000.	377.	0.249	0.216	907.	0.506
2000.	171.	0.248	0.267	829.	0.338
2000.	613.	0.498	0.183	838.	0.358
2000.	487.	0.497	0.239	781.	0.235
2000.	375.	0.498	0.276	714.	0.091
2000.	173.	0.502	0.368	621.	-0.109
2000.	615.	1.006	0.230	755.	0.179
2000.	486.	1.007	0.303	670.	-0.004
2000.	486.	0.996	0.297	668.	-0.008
2000.	378.	0.996	0.394	620.	-0.112
2000.	378.	0.999	0.396	620.	-0.112
2000.	173.	0.995	0.555	514.	-0.340
2000.	614.	1.508	0.304	738.	0.142
2000.	486.	1.502	0.410	653.	-0.041
2000.	375.	1.501	0.560	603.	-0.148
2000.	573.	2.008	0.376	687.	0.033
2000.	488.	2.003	0.520	647.	-0.053
2000.	379.	2.002	0.672	584.	-0.189
1200.	488.	0.248	0.193	964.	0.641
1200.	374.	0.248	0.229	939.	0.600
1200.	172.	0.247	0.294	900.	0.536
1200.	487.	0.497	0.322	883.	0.509
1200.	376.	0.498	0.367	826.	0.416
1200.	170.	0.500	0.452	723.	0.247
1200.	487.	1.003	0.423	745.	0.283
1200.	484.	0.995	0.431	739.	0.273
1200.	374.	0.996	0.526	698.	0.206
1200.	170.	0.999	0.629	555.	-0.027
1200.	486.	1.502	0.491	686.	0.187
1200.	376.	1.500	0.570	608.	0.059
1200.	486.	2.005	0.570	660.	0.144

TABLE NO.: 10
****

Z =	33.00
FP =	1.000
DH =	0.2599
Y =	1.
FG =	1.0068

TABLE :10- 1

PRESSURE P PSIA	INLET ENTHALPY HIN BTU/LB	MASS VELOCITY G LB/H/SQFT *1.E-6	MAXIMUM HEAT FLUX PHI BTU/H/SQFT *1.E-6	AV. EXIT ENTHALPY HEX BTU/LB	AV. STEAM QUALITY
**********	**********	**********	**********	**********	**********
2000.	602.	0.251	0.196	894.	0.478
2000.	482.	0.249	0.260	872.	0.431
2000.	383.	0.249	0.285	810.	0.298
2000.	176.	0.249	0.395	769.	0.209
2000.	597.	0.504	0.307	824.	0.328
2000.	488.	0.498	0.364	761.	0.192
2000.	377.	0.498	0.416	689.	0.037
2000.	613.	1.000	0.367	750.	0.168
2000.	599.	0.993	0.410	753.	0.175
2000.	485.	1.001	0.519	679.	0.015
2000.	378.	0.997	0.657	624.	-0.103
2000.	613.	1.499	0.463	729.	0.123
2000.	488.	1.500	0.681	658.	-0.030
2000.	617.	1.995	0.539	719.	0.102
2000.	485.	2.001	0.836	640.	-0.069
2000.	474.	2.011	0.802	623.	-0.105
2000.	615.	2.996	0.658	698.	0.056
2000.	488.	2.999	1.049	619.	-0.114
1600.	488.	0.496	0.376	771.	0.273
1600.	491.	0.999	0.488	675.	0.095
1600.	485.	1.999	0.804	636.	0.022
1600.	486.	2.995	0.957	606.	-0.033
1200.	489.	0.992	0.589	711.	0.228
1200.	376.	0.997	0.711	642.	0.115
1200.	490.	1.987	0.771	635.	0.104
1200.	489.	2.985	0.928	606.	0.056

TABLE NO.: 11
****

Z =	53.75
FP =	1.000
DH =	0.1752
Y =	1.
FG =	1.0287

TABLE :11- 1

PRESSURE P PSIA	INLET ENTHALPY HIN BTU/LB	MASS VELOCITY G LB/H/SQFT *1.E-6	MAXIMUM HEAT FLUX PHI BTU/H/SQFT *1.E-6	AV. EXIT ENTHALPY HEX BTU/LB	AV. STEAM QUALITY
**********	**********	**********	**********	**********	**********
2000.	171.	0.252	0.194	934.	0.565
2000.	378.	0.251	0.148	965.	0.632
2000.	488.	0.252	0.124	977.	0.657
2000.	615.	0.251	0.100	1011.	0.729
2000.	171.	0.503	0.301	765.	0.200
2000.	379.	0.503	0.222	818.	0.315
2000.	488.	0.503	0.189	860.	0.405
2000.	614.	0.504	0.153	916.	0.525
2000.	172.	1.006	0.481	646.	-0.055
2000.	375.	1.008	0.332	702.	0.065
2000.	378.	1.015	0.330	700.	0.060
2000.	489.	1.008	0.253	738.	0.141
2000.	488.	1.001	0.284	770.	0.211
2000.	488.	1.001	0.248	733.	0.132
2000.	612.	1.014	0.187	796.	0.266
2000.	614.	1.004	0.192	804.	0.284
2000.	488.	1.512	0.336	708.	0.079
2000.	615.	1.510	0.225	761.	0.193
2000.	189.	1.992	0.808	591.	-0.173
2000.	381.	2.002	0.596	676.	0.009
2000.	486.	2.005	0.436	701.	0.063
2000.	615.	2.015	0.261	744.	0.155
2000.	379.	2.991	0.800	645.	-0.059
2000.	488.	3.014	0.603	687.	0.032
2000.	618.	3.029	0.365	738.	0.141
2000.	377.	3.990	0.926	607.	-0.141
2000.	488.	4.005	0.740	671.	-0.002
1600.	486.	0.248	0.131	1009.	0.715
1600.	485.	0.498	0.212	907.	0.526
1600.	488.	1.005	0.308	792.	0.312
1600.	488.	2.004	0.455	713.	0.165
1600.	487.	3.008	0.566	674.	0.093
1200.	170.	0.251	0.208	989.	0.682
1200.	376.	0.251	0.163	1018.	0.728
1200.	483.	0.252	0.138	1028.	0.746
1200.	169.	0.501	0.346	854.	0.461
1200.	377.	0.501	0.292	954.	0.624
1200.	486.	0.503	0.242	963.	0.639
1200.	178.	1.003	0.550	722.	0.246
1200.	376.	0.998	0.428	802.	0.375
1200.	489.	1.004	0.356	840.	0.438
1200.	374.	2.002	0.631	686.	0.187
1200.	487.	2.000	0.477	723.	0.248
1200.	378.	2.999	0.779	635.	0.104
1200.	489.	2.995	0.587	682.	0.180

TABLE NO.: 12
****

Z =	53.75
FP =	1.000
DH =	0.1752
Y =	1.
FG =	1.0287

TABLE :12- 1

PRESSURE P PSIA	INLET ENTHALPY HIN BTU/LB	MASS VELOCITY G LB/H/SQFT *1.E-6	MAXIMUM HEAT FLUX PHI BTU/H/SQFT *1.E-6	AV. EXIT ENTHALPY HEX BTU/LB	AV. STEAM QUALITY
**********	**********	**********	**********	**********	**********
2000.	170.	0.252	0.205	977.	0.656
2000.	380.	0.252	0.163	1020.	0.749
2000.	487.	0.252	0.136	1016.	0.741
2000.	585.	0.257	0.116	1035.	0.781
2000.	172.	0.504	0.298	759.	0.189
2000.	379.	0.504	0.257	886.	0.461
2000.	487.	0.506	0.216	909.	0.511
2000.	603.	0.509	0.171	937.	0.572
2000.	174.	1.007	0.495	661.	-0.024
2000.	375.	1.001	0.401	772.	0.216
2000.	375.	1.003	0.392	762.	0.194
2000.	488.	1.007	0.303	786.	0.246
2000.	488.	1.002	0.322	806.	0.289
2000.	608.	1.018	0.214	817.	0.312
2000.	605.	1.013	0.208	809.	0.295
2000.	484.	1.502	0.414	757.	0.183
2000.	606.	1.523	0.274	784.	0.242
2000.	379.	2.000	0.635	694.	0.047
2000.	484.	2.007	0.504	733.	0.131
2000.	616.	2.011	0.319	773.	0.218
2000.	485.	3.010	0.656	701.	0.062
2000.	606.	3.034	0.446	752.	0.172
1600.	483.	0.252	0.139	1032.	0.756
1600.	486.	0.501	0.245	971.	0.645
1600.	485.	1.006	0.345	825.	0.373
1600.	484.	2.002	0.492	728.	0.193
1600.	483.	3.010	0.631	691.	0.125
1200.	170.	0.252	0.210	998.	0.696
1200.	376.	0.253	0.163	1015.	0.724
1200.	373.	0.253	0.168	1032.	0.752
1200.	484.	0.251	0.137	1024.	0.738
1200.	171.	0.502	0.366	894.	0.527
1200.	376.	0.504	0.297	961.	0.636
1200.	372.	0.505	0.300	962.	0.637
1200.	487.	0.501	0.255	992.	0.686
1200.	167.	1.006	0.600	758.	0.304
1200.	373.	1.006	0.467	833.	0.428
1200.	381.	1.004	0.457	832.	0.426
1200.	485.	1.006	0.387	866.	0.481
1200.	486.	0.998	0.377	861.	0.473
1200.	378.	1.997	0.651	701.	0.211
1200.	488.	1.999	0.484	728.	0.255
1200.	376.	2.997	0.809	644.	0.118
1200.	484.	3.006	0.591	679.	0.176
800.	377.	0.252	0.158	997.	0.706
800.	376.	0.501	0.310	989.	0.696
800.	378.	1.004	0.476	848.	0.491
800.	375.	1.997	0.693	719.	0.304
400.	163.	0.252	0.203	963.	0.689
400.	372.	0.250	0.157	995.	0.731
400.	163.	0.504	0.375	901.	0.610
400.	373.	0.501	0.299	965.	0.692
400.	167.	1.004	0.610	770.	0.443
400.	375.	1.006	0.457	825.	0.514
400.	374.	1.848	0.534	661.	0.303

TABLE :12- 2

PRESSURE P PSIA	INLET ENTHALPY HIN BTU/LB	MASS VELOCITY G LB/H/SQFT *1.E-6	MAXIMUM HEAT FLUX PHI BTU/H/SQFT *1.E-6	AV. EXIT ENTHALPY HEX BTU/LB	AV. STEAM QUALITY
**********	**********	**********	**********	**********	**********
2000.	373.	0.050	0.044	1116.	0.957
2000.	471.	0.050	0.039	1114.	0.952
2000.	489.	0.050	0.038	1102.	0.925
2000.	378.	0.100	0.072	1032.	0.775
2000.	489.	0.100	0.064	1056.	0.827
2000.	592.	0.101	0.054	1055.	0.825
2000.	380.	0.175	0.115	1030.	0.771
2000.	488.	0.176	0.102	1024.	0.758
2000.	598.	0.178	0.083	1023.	0.757
1200.	374.	0.050	0.044	1153.	0.949
1200.	469.	0.050	0.039	1159.	0.959
1200.	374.	0.112	0.080	1044.	0.771
1200.	487.	0.100	0.065	1092.	0.849
1200.	376.	0.175	0.112	984.	0.673
1200.	487.	0.174	0.093	992.	0.687

TABLE NO.: 13
****

Z =	93.75
FP =	1.114
DH =	0.2335
Y =	1.
FG =	1.0006

TABLE :13- 1

PRESSURE P PSIA	INLET ENTHALPY HIN BTU/LB	MASS VELOCITY G LB/H/SQFT *1.E-6	MAXIMUM HEAT FLUX PHI BTU/H/SQFT *1.E-6	AV. EXIT ENTHALPY HEX BTU/LB	AV. STEAM QUALITY
**********	**********	**********	**********	**********	**********
2000.	173.	0.101	0.100	1079.	0.877
2000.	378.	0.101	0.078	1081.	0.881
2000.	487.	0.101	0.067	1091.	0.903
2000.	175.	0.176	0.155	976.	0.656
2000.	376.	0.177	0.123	1011.	0.731
2000.	488.	0.177	0.103	1016.	0.740
2000.	608.	0.177	0.081	1021.	0.752
2000.	173.	0.252	0.199	893.	0.477
2000.	377.	0.252	0.156	943.	0.584
2000.	488.	0.252	0.129	955.	0.611
2000.	607.	0.254	0.103	977.	0.656
2000.	222.	0.503	0.238	656.	-0.034
2000.	382.	0.503	0.211	766.	0.203
2000.	484.	0.503	0.168	789.	0.253
2000.	486.	0.504	0.175	803.	0.282
2000.	559.	0.507	0.145	820.	0.319
2000.	618.	0.505	0.129	851.	0.386
2000.	221.	1.003	0.349	539.	-0.285
2000.	372.	1.005	0.267	622.	-0.108
2000.	485.	1.004	0.221	686.	0.031
2000.	487.	1.004	0.227	694.	0.047
2000.	561.	1.003	0.182	727.	0.118
2000.	617.	1.006	0.164	766.	0.202
2000.	380.	1.504	0.347	590.	-0.176
2000.	381.	1.504	0.342	589.	-0.179
2000.	485.	1.507	0.277	652.	-0.043
2000.	486.	1.505	0.279	656.	-0.035
2000.	487.	1.507	0.281	657.	-0.032
2000.	559.	1.509	0.219	691.	0.042
2000.	616.	1.509	0.189	731.	0.127
2000.	387.	2.013	0.421	578.	-0.203
2000.	489.	2.006	0.327	638.	-0.074
2000.	491.	2.001	0.338	645.	-0.058
2000.	559.	2.013	0.262	677.	0.012
2000.	614.	1.892	0.208	715.	0.092
1600.	378.	0.101	0.080	1095.	0.874
1600.	377.	0.176	0.123	1016.	0.727
1600.	173.	0.252	0.203	909.	0.528
1600.	376.	0.252	0.159	950.	0.605
1600.	487.	0.252	0.133	970.	0.642
1600.	222.	0.500	0.273	718.	0.175
1600.	377.	0.505	0.219	772.	0.275
1600.	489.	0.501	0.181	818.	0.360
1600.	559.	0.503	0.163	856.	0.430
1600.	224.	1.000	0.358	550.	-0.137
1600.	377.	1.004	0.303	652.	0.051
1600.	485.	1.003	0.253	716.	0.170
1600.	564.	1.001	0.218	762.	0.255
1600.	377.	1.503	0.363	598.	-0.049
1600.	486.	1.503	0.308	674.	0.092
1600.	562.	1.499	0.242	710.	0.159
1600.	381.	2.005	0.423	574.	-0.093
1600.	486.	2.023	0.344	642.	0.034
1600.	562.	1.971	0.269	686.	0.116
1200.	377.	0.101	0.078	1087.	0.842

TABLE :13- 2

PRESSURE P PSIA	INLET ENTHALPY HIN BTU/LB	MASS VELOCITY G LB/H/SQFT *1.E-6	MAXIMUM HEAT FLUX PHI BTU/H/SQFT *1.E-6	AV. EXIT ENTHALPY HEX BTU/LB	AV. STEAM QUALITY
**********	**********	**********	**********	**********	**********
1200.	376.	0.176	0.122	1007.	0.710
1200.	373.	0.252	0.159	951.	0.620
1200.	487.	0.251	0.137	986.	0.677
1200.	221.	0.500	0.277	726.	0.252
1200.	376.	0.499	0.221	779.	0.338
1200.	489.	0.498	0.195	845.	0.446
1200.	227.	1.002	0.422	611.	0.064
1200.	374.	1.001	0.336	680.	0.177
1200.	486.	0.999	0.281	743.	0.280
1200.	401.	1.497	0.422	659.	0.142
1200.	485.	1.502	0.332	686.	0.187
1200.	459.	1.994	0.423	653.	0.132
1200.	487.	2.000	0.375	658.	0.141

TABLE NO.: 14
****

Z =	93.75
FP =	1.091
DH =	0.1104
Y =	1.
FG =	0.8878

TABLE :14- 1

PRESSURE P PSIA	INLET ENTHALPY HIN BTU/LB	MASS VELOCITY G LB/H/SQFT *1.E-6	MAXIMUM HEAT FLUX PHI BTU/H/SQFT *1.E-6	AV. EXIT ENTHALPY HEX BTU/LB	AV. STEAM QUALITY
**********	**********	**********	**********	**********	**********
2000.	620.	0.149	0.037	981.	0.666
2000.	378.	0.150	0.060	956.	0.612
2000.	171.	0.151	0.077	909.	0.511
2000.	619.	0.251	0.047	888.	0.465
2000.	490.	0.252	0.060	836.	0.354
2000.	381.	0.251	0.075	815.	0.308
2000.	176.	0.251	0.097	733.	0.132
2000.	620.	0.504	0.061	794.	0.263
2000.	490.	0.501	0.081	724.	0.112
2000.	379.	0.501	0.096	657.	-0.032
2000.	377.	0.501	0.099	663.	-0.019
2000.	173.	0.500	0.137	568.	-0.224
2000.	614.	0.754	0.076	760.	0.190
2000.	487.	0.755	0.099	677.	0.011
2000.	376.	0.754	0.121	609.	-0.135
2000.	176.	0.753	0.176	514.	-0.340
2000.	617.	0.985	0.098	760.	0.190
2000.	489.	0.994	0.121	665.	-0.015
2000.	380.	1.001	0.151	598.	-0.159
2000.	379.	1.003	0.152	598.	-0.159
2000.	175.	0.998	0.209	479.	-0.415
2000.	614.	1.482	0.122	733.	0.132
2000.	487.	1.490	0.167	649.	-0.049
2000.	381.	1.504	0.205	578.	-0.202
2000.	173.	1.404	0.268	449.	-0.480
2000.	613.	1.980	0.146	720.	0.104
2000.	487.	1.982	0.207	638.	-0.073
2000.	376.	2.000	0.271	572.	-0.215
2000.	170.	1.996	0.384	449.	-0.480
2000.	489.	2.970	0.286	631.	-0.088
2000.	378.	3.000	0.372	558.	-0.245
2000.	610.	2.850	0.207	715.	0.093
1600.	491.	0.250	0.065	868.	0.453
1600.	381.	0.247	0.079	843.	0.406
1600.	489.	0.503	0.086	737.	0.210
1600.	382.	0.499	0.098	664.	0.074
1600.	179.	0.509	0.138	571.	-0.098
1600.	490.	0.991	0.136	689.	0.121
1600.	377.	0.998	0.153	598.	-0.048
1600.	488.	1.487	0.178	661.	0.069
1600.	378.	1.492	0.207	578.	-0.085
1600.	485.	1.988	0.207	636.	0.022
1600.	377.	1.990	0.258	565.	-0.109
1200.	489.	0.250	0.067	879.	0.502
1200.	378.	0.250	0.079	835.	0.430
1200.	175.	0.251	0.111	809.	0.388
1200.	486.	0.500	0.090	738.	0.272
1200.	377.	0.500	0.112	702.	0.213
1200.	175.	0.501	0.136	566.	-0.009
1200.	490.	0.778	0.131	734.	0.265
1200.	380.	0.750	0.136	642.	0.115
1200.	488.	0.995	0.155	712.	0.229
1200.	376.	0.994	0.177	633.	0.100
1200.	488.	1.488	0.195	677.	0.172
1200.	380.	1.490	0.217	591.	0.032

TABLE :14- 2

PRESSURE P PSIA	INLET ENTHALPY HIN BTU/LB	MASS VELOCITY G LB/H/SQFT *1.E-6	MAXIMUM HEAT FLUX PHI BTU/H/SQFT *1.E-6	AV. EXIT ENTHALPY HEX BTU/LB	AV. STEAM QUALITY
**********	**********	**********	**********	**********	**********
1200.	489.	1.987	0.229	655.	0.136
1200.	376.	1.987	0.246	555.	-0.027
1200.	174.	1.994	0.387	454.	-0.192
1200.	485.	2.980	0.294	628.	0.092
1200.	383.	2.970	0.339	548.	-0.039

TABLE NO.: 15
****

Z =	17.00
FP =	1.000
DH =	0.0903
Y =	1.
FG =	1.0000

TABLE :15- 1

PRESSURE P PSIA	INLET ENTHALPY HIN BTU/LB	MASS VELOCITY G LB/H/SQFT *1.E-6	MAXIMUM HEAT FLUX PHI BTU/H/SQFT *1.E-6	AV. EXIT ENTHALPY HEX BTU/LB	AV. STEAM QUALITY
**********	**********	**********	**********	**********	**********
1200.	362.	0.490	0.310	748.	0.288
1200.	404.	0.500	0.308	779.	0.338
1200.	453.	0.510	0.293	809.	0.388
1200.	509.	0.480	0.284	867.	0.483
1200.	571.	0.510	0.269	894.	0.527
1200.	555.	0.990	0.391	796.	0.366
1200.	502.	1.010	0.455	777.	0.335
1200.	457.	1.060	0.485	737.	0.270
1200.	405.	0.990	0.504	715.	0.234
1200.	358.	1.020	0.524	671.	0.162
1200.	295.	0.990	0.530	622.	0.082
1200.	349.	1.990	0.690	560.	-0.019
1200.	398.	1.910	0.766	641.	0.114
1200.	455.	1.950	0.736	685.	0.186
1200.	484.	2.030	0.700	694.	0.200
1200.	517.	2.060	0.607	697.	0.205
1200.	549.	2.000	0.502	703.	0.214
1200.	542.	3.000	0.612	667.	0.156
1200.	485.	2.000	0.658	687.	0.188
1200.	455.	2.030	0.734	676.	0.170
1200.	511.	2.880	0.700	660.	0.145
1200.	467.	2.960	0.860	643.	0.117
1200.	415.	3.020	0.929	603.	0.051
1200.	394.	2.920	0.948	592.	0.034
1200.	444.	2.930	0.889	629.	0.093
1200.	495.	2.920	0.773	654.	0.135
1200.	527.	2.990	0.680	667.	0.155
1200.	189.	0.520	0.336	583.	0.018
1200.	345.	2.050	0.732	563.	-0.014
1200.	362.	1.990	0.801	607.	0.058
1200.	452.	4.000	1.025	609.	0.061
1200.	471.	3.740	0.962	629.	0.094
1200.	495.	3.800	0.915	641.	0.113
1200.	508.	3.700	0.850	648.	0.125
1200.	520.	3.650	0.781	651.	0.130
1200.	542.	3.440	0.695	666.	0.154
1200.	477.	3.560	0.941	638.	0.108
1200.	415.	4.000	1.175	594.	0.036
1200.	386.	4.090	1.280	576.	0.007
1200.	415.	3.000	0.958	609.	0.061
1200.	482.	2.970	0.818	650.	0.128
1200.	535.	2.990	0.655	670.	0.160
1200.	530.	3.520	0.724	655.	0.137
1200.	522.	2.030	0.559	692.	0.196